

SU(2) gauge theory of the pseudogap phase in the two-dimensional Hubbard model

Pietro M. Bonetti¹ and Walter Metzner¹

¹*Max Planck Institute for Solid State Research, Heisenbergstrasse 1, D-70569 Stuttgart, Germany*
(Dated: July 5, 2022)

We present a SU(2) gauge theory of fluctuating magnetic order in the two-dimensional Hubbard model. The theory is based on a fractionalization of electrons in fermionic chargons and bosonic spinons. The chargons undergo Néel or spiral magnetic order below a density dependent transition temperature T^* . Fluctuations of the spin orientation are described by a non-linear sigma model obtained from a gradient expansion of the spinon action. The spin stiffnesses are computed from a renormalization group improved random phase approximation. Our approximations are applicable for a weak or moderate Hubbard interaction. The spinon fluctuations prevent magnetic long-range order of the electrons at any finite temperature. The phase with magnetic chargon order exhibits many features characterizing the pseudogap regime in high- T_c cuprates: a strong reduction of charge carrier density, a spin gap, Fermi arcs, and electronic nematicity.

I. INTRODUCTION

Besides their exceptionally high transition temperatures for superconductivity, a peculiar and fairly universal feature of hole-doped cuprate superconductors is their pseudogap behavior for temperatures above T_c , observed in a broad doping range from the underdoped into the optimally doped regime [1, 2]. The pseudogap behavior sets in at a temperature T^* which is much higher than T_c in the underdoped regime, and merges with T_c near optimal doping. It is characterized by a spin gap, a reduction of the charge carrier concentration, a suppression of the electronic density of states, a gap for single-particle excitations in the antinodal region of the Brillouin zone, and a reconstructed Fermi surface which in photoemission looks like Fermi arcs. It is also associated with a tendency to electronic nematicity, where the electronic state breaks the tetragonal symmetry of the crystal. Suppressing superconductivity by high magnetic fields, the pseudogap regime extends into the region which in the absence of magnetic fields is superconducting – for doping concentrations as high as about 20 percent [2].

There is convincing numerical evidence for pseudogap behavior in the strongly interacting two-dimensional Hubbard model, in particular from quantum cluster calculations [3]. An unbiased “fluctuation diagnostics” [4] of the contributions to the self-energy has revealed that the pseudogap is generated predominantly by antiferromagnetic fluctuations, that is, by spin fluctuations with wave vectors at or near (π, π) .

While the guidance provided by numerical results is clearly very valuable, a deeper understanding of the pseudogap phenomenon and data with a higher momentum resolution remain desirable. The momentum resolution of the self-energy and of other momentum dependent quantities is limited in all cluster methods, since the computational effort grows exponentially with the cluster size. Also long-range correlations (in real space) beyond the cluster size cannot be captured. The same limitations hold of course for direct numerical simulations of finite systems.

In this situation approximate analytic theories can provide further insights, especially concerning long-range correlations and the fine-structure in momentum space. Early theories of the pseudogap phenomenon were based on weak-coupling diagrammatic perturbation expansions, most notably Moriya’s renormalized theory [5] and the two-particle self-consistent theory by Vilk and Tremblay [6]. The Mermin-Wagner theorem on the absence of spin symmetry breaking at finite temperatures is respected in these theories, but the pseudogap seems to develop only for fairly large magnetic correlation lengths, while the numerical data show that strong short-ranged correlations are sufficient.

More recently it was shown by Sachdev, Scheurer, and coworkers that many features of the pseudogap behavior observed in cuprates can be captured by a SU(2) gauge theory [7–11]. This approach is based on a fractionalization of the electron into a fermionic “chargon” and a charge neutral “spinon”. The latter is a SU(2) matrix providing a space and time dependent local reference frame [12]. The local spin rotations can be parametrized by a SU(2) gauge field, and the fractionalization leads to a gauge redundancy. One can then consider states where the chargons exhibit some sort of magnetic order (for example, Néel or spiral), while the spinon fluctuations prevent symmetry breaking and magnetic long-range order of the physical spin-carrying electrons [13–15]. Quantities involving only charge degrees of freedom behave essentially as in a conventional magnetically ordered state, and the Fermi surface gets correspondingly reconstructed. While long-range order is absent, at least at finite temperatures, the electrons are subject to a “topological” order in the sense that smoothly varying local spin rotations can map the fluctuating spin configurations to an ordered pattern, that is, there is no proliferation of topological defects [11].

In this paper we formulate a SU(2) gauge theory for the fluctuating antiferromagnet in a way that allows us to compute, in a decent approximation for weak or moderate Hubbard interactions, effective low-energy parameters and physical quantities as a function of the microscopic model parameters. The chargon order parameter

is computed from a renormalized mean-field theory [16] which takes high energy (above T^*) spin, charge, and pairing fluctuations into account on equal footing. We allow for Néel and planar spiral order with generally incommensurate ordering wave vectors. The spinon dynamics is described by a non-linear sigma model (NL σ M). The parameters of the NL σ M, that is, the spin stiffnesses, are computed from a renormalized RPA for the SU(2) gauge field response of the chargons [17], and the ultraviolet cutoff is estimated via the magnetic coherence length. The NL σ M is evaluated in a large N expansion. Applying the general theory to the Hubbard model with next and next-nearest neighbor hopping at a moderate interaction strength (about half band width), we obtain a broad finite temperature pseudogap regime on the hole doped side and a narrower pseudogap region for electron doping. Nematic order is present at sufficiently low temperatures for hole doping, but not for electron doping. There is no magnetic long-range order at $T > 0$, in agreement with the Mermin-Wagner theorem, and the spin excitations are gapped. The spinon quantum fluctuations are not strong enough to destroy magnetic long-range order in the ground state, except possibly near the edge of the pseudogap regime at large hole doping. In the hole doped pseudogap regime, the Fermi surfaces extracted from the single-particle spectral function have the form of hole pocket boundaries with a truncated back side. Their topology is thus the same as for the experimentally observed Fermi arcs.

The paper is structured as follows. In Sec. II we derive the general structure of the SU(2) gauge theory for the pseudogap phase with Néel or spiral order in the chargin sector. In Sec. III we describe how we compute the parameters of the gauge theory, in particular the spin stiffnesses, from the underlying microscopic model. Sec. IV deals with the solution of the nonlinear sigma model for the spinon fluctuations in a large N expansion. Results for the two-dimensional Hubbard model are presented in Sec. V. We conclude with a summary and a final discussion of our theory in Sec. VI.

II. SU(2) GAUGE THEORY

A. Fractionalizing the electron field

We consider the Hubbard model on a square lattice with units of length such that the lattice spacing is one. The Hubbard action in imaginary time reads

$$\mathcal{S}[c, c^*] = \int_0^\beta d\tau \left\{ \sum_{j,j',\sigma} c_{j\sigma}^* [(\partial_\tau - \mu) \delta_{jj'} + t_{jj'}] c_{j'\sigma} + U \sum_j n_{j\uparrow} n_{j\downarrow} \right\}, \quad (1)$$

where $c_{j\sigma} = c_{j\sigma}(\tau)$ and $c_{j\sigma}^* = c_{j\sigma}^*(\tau)$ are Grassmann fields corresponding to the annihilation and creation, respectively, of an electron with spin orientation σ at site

j , and $n_{j\sigma} = c_{j\sigma}^* c_{j\sigma}$. The chemical potential is denoted by μ , and $U > 0$ is the strength of the (repulsive) Hubbard interaction. To simplify the notation, we write the dependence of the fields on the imaginary time τ only if needed for clarity.

The action in (1) is invariant under *global* SU(2) rotations acting on the Grassmann fields as

$$c_j \rightarrow \mathcal{U} c_j, \quad c_j^* \rightarrow c_j^* \mathcal{U}^\dagger, \quad (2)$$

where c_j and c_j^* are two-component spinors composed from $c_{j\sigma}$ and $c_{j\sigma}^*$, respectively, while \mathcal{U} is a SU(2) matrix acting in spin space.

To separate collective spin fluctuations from the charge degrees of freedom, we fractionalize the electronic fields as [12–15]

$$c_j = R_j \psi_j, \quad c_j^* = \psi_j^* R_j^\dagger, \quad (3)$$

where $R_j \in \text{SU}(2)$, to which we refer as “spinon”, is composed of bosonic fields, and the components ψ_{js} of the “chargin” spinor ψ_j are fermionic. According to (2) and (3) the spinons transform under the global SU(2) spin rotation by a *left* matrix multiplication, while the chargons are left invariant. Conversely, a U(1) charge transformation acts only on ψ_j , leaving R_j unaffected. We have therefore separated the spin degrees of freedom of the physical electrons, now encoded in the spinons, from their charge, carried by the chargons. The transformation in Eq. (3) introduces a redundant SU(2) gauge symmetry, acting as

$$\psi_j \rightarrow \mathcal{V}_j \psi_j, \quad \psi_j^* \rightarrow \psi_j^* \mathcal{V}_j^\dagger, \quad (4a)$$

$$R_j \rightarrow R_j \mathcal{V}_j^\dagger, \quad R_j^\dagger \rightarrow \mathcal{V}_j R_j^\dagger, \quad (4b)$$

with $\mathcal{V}_j \in \text{SU}(2)$. Hence, the components ψ_{js} of ψ_j carry a SU(2) gauge index s , while the components $R_{j,\sigma s}$ of R_j have two indices, the first one (σ) corresponding to the global SU(2) symmetry, and the second one (s) to SU(2) gauge transformations.

We now rewrite the Hubbard action in terms of the spinon and chargin fields. The quadratic part of (1) can be expressed as [14]

$$\mathcal{S}_0[\psi, \psi^*, R] = \int_0^\beta d\tau \left\{ \sum_j \psi_j^* [\partial_\tau - \mu - A_{0,j}] \psi_j + \sum_{j,j'} t_{jj'} \psi_j^* e^{-\mathbf{r}_{jj'} \cdot (\nabla - i\mathbf{A}_j)} \psi_j \right\}, \quad (5)$$

where we have introduced a SU(2) gauge field, defined as

$$A_{\mu,j} = (A_{0,j}, \mathbf{A}_j) = iR_j^\dagger \partial_\mu R_j, \quad (6)$$

with $\partial_\mu = (i\partial_\tau, \nabla)$. Here, the nabla operator ∇ is defined as generator of translations on the lattice, that is, $e^{-\mathbf{r}_{jj'} \cdot \nabla}$ with $\mathbf{r}_{jj'} = \mathbf{r}_j - \mathbf{r}_{j'}$ is the translation operator from site j to site j' .

To rewrite the interacting part in (1), we use the decomposition [12, 14, 18]

$$n_{j\uparrow}n_{j\downarrow} = \frac{1}{4}(n_j)^2 - \frac{1}{4}(c_j^* \vec{\sigma} \cdot \hat{\Omega}_j c_j)^2, \quad (7)$$

where $n_j = n_{j,\uparrow} + n_{j,\downarrow}$ is the charge density operator, $\vec{\sigma} = (\sigma^1, \sigma^2, \sigma^3)$ are the Pauli matrices, and $\hat{\Omega}_j$ is an arbitrary time- and site-dependent unit vector. Inserting the decomposition (3), the interaction term of the Hubbard action can therefore be written as

$$\mathcal{S}_{\text{int}}[\psi, \psi^*, R] = \int_0^\beta d\tau U \sum_j \left[\frac{1}{4}(n_j^\psi)^2 - \frac{1}{4}(\vec{S}_j^\psi \cdot \hat{\Omega}_j^R)^2 \right], \quad (8)$$

where $n_j^\psi = \psi_j^* \psi_j$ is the chargin density operator, $\vec{S}_j^\psi = \frac{1}{2} \psi_j^* \vec{\sigma} \psi_j$ is the chargin spin operator, and $\hat{\Omega}_j^R$ is a unit vector obtained by rotating $\hat{\Omega}_j$ as

$$\vec{\sigma} \cdot \hat{\Omega}_j^R = R_j^\dagger \vec{\sigma} \cdot \hat{\Omega}_j R_j. \quad (9)$$

Using (7) again, we obtain

$$\mathcal{S}_{\text{int}}[\psi, \psi^*, R] = \int_0^\beta d\tau U \sum_j n_{j\uparrow}^\psi n_{j\downarrow}^\psi, \quad (10)$$

with $n_{js}^\psi = \psi_{js}^* \psi_{js}$. Therefore, the final form of the action $\mathcal{S} = \mathcal{S}_0 + \mathcal{S}_{\text{int}}$ is nothing but the Hubbard model action where the physical electrons have been replaced by chargons coupled to a SU(2) gauge field.

Since the chargons do not carry the physical spin degree of freedom, a global breaking of their SU(2) gauge symmetry ($\langle \vec{S}_j^\psi \rangle \neq 0$) does not necessarily imply long range order for the electrons. The matrices R_j describe directional fluctuations of the order parameter $\langle \vec{S}_j^\psi \rangle$, where, at low temperatures, the most important ones vary slowly in space and time.

B. Nonlinear sigma model

We now derive a low energy effective action for the spinon fields R_j by integrating out the chargons,

$$e^{-\mathcal{S}_{\text{eff}}[R]} = \int \mathcal{D}\psi \mathcal{D}\psi^* e^{-\mathcal{S}[\psi, \psi^*, R]}. \quad (11)$$

Since the action \mathcal{S} is quartic in the fermionic fields, the functional integral must be carried out by means of an approximate method. In previous works [12–14] a Hubbard-Stratonovich transformation has been applied to decouple the chargin interaction, together with a saddle point approximation on the auxiliary bosonic (Higgs) field. We will employ an improved approximation based on the functional renormalization group [19], which we describe in Sec. III.

The effective action for the spinons can be obtained by computing the response functions of the chargons to

a fictitious SU(2) gauge field. Since we assign only low energy long wave length fluctuations to the spinons in the decomposition (3), the spinon field R_j is slowly varying in space and time. Hence, we can perform a gradient expansion. To second order in the gradient $\partial_\mu R_j$, the effective action $\mathcal{S}_{\text{eff}}[R]$ has the general form

$$\mathcal{S}_{\text{eff}}[R] = \int_{\mathcal{T}} dx \left[\mathcal{B}_\mu^a A_\mu^a(x) + \frac{1}{2} \mathcal{J}_{\mu\nu}^{ab} A_\mu^a(x) A_\nu^b(x) \right], \quad (12)$$

where $x = (\tau, \mathbf{r})$ combines imaginary time and space coordinates, $\mathcal{T} = [0, \beta] \times \mathbb{R}^2$ is the integration region, and repeated indices are summed. We have expanded the gauge field A_μ in terms of the SU(2) generators,

$$A_\mu(x) = A_\mu^a(x) \sigma^a / 2, \quad (13)$$

with a running from 1 to 3. In line with the gradient expansion, the gauge field is now defined over a *continuous* space-time. The coefficients in (12) do not depend on x and are given by

$$\mathcal{B}_\mu^a = \frac{1}{2} \sum_{j,j'} \gamma_\mu^{(1)}(j, j') \langle \psi_j^*(0) \sigma^a \psi_{j'}(0) \rangle, \quad (14)$$

$$\begin{aligned} \mathcal{J}_{\mu\nu}^{ab} &= -\frac{1}{4} \sum_{j,j'} \sum_{l,l'} \gamma_\mu^{(1)}(j, j') \gamma_\nu^{(1)}(l, l') \\ &\quad \times \int_0^\beta d\tau \langle (\psi_j^*(\tau) \sigma^a \psi_{j'}(\tau)) (\psi_l^*(0) \sigma^b \psi_{l'}(0)) \rangle_c \\ &\quad + \frac{1}{4} \sum_{j,j'} \gamma_{\mu\nu}^{(2)}(j, j') \langle \psi_j^*(0) \psi_{j'}(0) \rangle \delta_{ab}, \end{aligned} \quad (15)$$

where $\langle \bullet \rangle$ ($\langle \bullet \rangle_c$) denotes the (connected) average with respect to the chargin Hubbard action. The first and second order current vertices have been defined as

$$\gamma^{(1)}(j, j') = (\delta_{jj'}, i x_{jj'} t_{jj'}, i y_{jj'} t_{jj'}), \quad (16a)$$

$$\gamma^{(2)}(j, j') = - \begin{pmatrix} 0 & 0 & 0 \\ 0 & x_{jj'} x_{jj'} t_{jj'} & x_{jj'} y_{jj'} t_{jj'} \\ 0 & y_{jj'} x_{jj'} t_{jj'} & y_{jj'} y_{jj'} t_{jj'} \end{pmatrix}, \quad (16b)$$

where $x_{jj'}$ and $y_{jj'}$ are the x and y components, respectively of $\mathbf{r}_{jj'} = \mathbf{r}_j - \mathbf{r}_{j'}$.

In Appendix A we will see that the linear term in (12) vanishes. We therefore consider only the quadratic contribution to the effective action. Defining the adjoint representation \mathcal{R} of the SU(2) rotation R via

$$R^\dagger \sigma^a R = \mathcal{R}^{ab} \sigma^b, \quad (17)$$

we obtain the non-linear sigma model (NL σ M) action for the directional fluctuations (see Appendix B)

$$\mathcal{S}_{\text{NL}\sigma\text{M}}[\mathcal{R}] = \int_{\mathcal{T}} dx \frac{1}{2} \text{Tr} [\mathcal{P}_{\mu\nu} (\partial_\mu \mathcal{R}^T) (\partial_\nu \mathcal{R})], \quad (18)$$

where $\mathcal{P}_{\mu\nu} = \frac{1}{2} \text{Tr} [\mathcal{J}_{\mu\nu}] \mathbb{1} - \mathcal{J}_{\mu\nu}$.

The structure of the matrices $\mathcal{J}_{\mu\nu}$ and $\mathcal{P}_{\mu\nu}$ depends on the magnetically ordered chargin state. In the trivial

case $\langle \vec{S}_j^\psi \rangle = 0$ all the stiffnesses vanish and no meaningful low energy theory for R can be derived. A well-defined low energy theory emerges, for example, when *Néel* antiferromagnetic order is realized in the chargon sector, that is,

$$\langle \vec{S}_j^\psi \rangle \propto (-1)^{r_j} \hat{u}, \quad (19)$$

where \hat{u} is an arbitrary fixed unit vector. Choosing $\hat{u} = \hat{e}_1 = (1, 0, 0)$, the spin stiffness matrix in the Néel state has the form

$$\mathcal{J}_{\mu\nu} = \begin{pmatrix} 0 & 0 & 0 \\ 0 & J_{\mu\nu} & 0 \\ 0 & 0 & J_{\mu\nu} \end{pmatrix}, \quad (20)$$

with $(J_{\mu\nu}) = \text{diag}(-Z, J, J)$. In this case the effective theory reduces to the well-known $O(3)/O(2) \simeq S_2$ nonlinear sigma model [20, 21]

$$\mathcal{S}_{\text{NL}\sigma\text{M}} = \frac{1}{2} \int_{\mathcal{T}} dx \left(Z |\partial_\tau \hat{\Omega}|^2 + J |\vec{\nabla} \hat{\Omega}|^2 \right), \quad (21)$$

where $\hat{\Omega}^a = \mathcal{R}^{a1}$, and $|\hat{\Omega}|^2 = 1$.

Another possibility is planar *spiral* magnetic ordering of the chargons,

$$\langle \vec{S}_j^\psi \rangle \propto \cos(\mathbf{Q} \cdot \mathbf{r}_j) \hat{u}_1 + \sin(\mathbf{Q} \cdot \mathbf{r}_j) \hat{u}_2, \quad (22)$$

where \mathbf{Q} is a fixed wave vector as obtained by minimizing the chargon free energy, while \hat{u}_1 and \hat{u}_2 are two arbitrary mutually orthogonal unit vectors. The special case $\mathbf{Q} = (\pi, \pi)$ corresponds to the Néel state. Fixing \hat{u}_1 to \hat{e}_1 and \hat{u}_2 to $\hat{e}_2 \equiv (0, 1, 0)$, the spin stiffness matrix assumes the form

$$\mathcal{J}_{\mu\nu} = \begin{pmatrix} J_{\mu\nu}^\perp & 0 & 0 \\ 0 & J_{\mu\nu}^\perp & 0 \\ 0 & 0 & J_{\mu\nu}^\square \end{pmatrix}, \quad (23)$$

where

$$(J_{\mu\nu}^a) = \begin{pmatrix} -Z^a & 0 & 0 \\ 0 & J_{xx}^a & J_{xy}^a \\ 0 & J_{yx}^a & J_{yy}^a \end{pmatrix}. \quad (24)$$

for $a \in \{\perp, \square\}$. In this case, the effective action maintains its general form (18) and it describes the $O(3) \times O(2)/O(2)$ symmetric NL σ M, which has been previously studied in the context of geometrically frustrated antiferromagnets [22–26]. This theory has three independent degrees of freedom, corresponding to one *in-plane* and two *out-of-plane* Goldstone modes.

In the following we will restrict the magnetic ordering pattern of the chargons to Néel or planar spiral order. Néel or spiral antiferromagnetism has been found in the two-dimensional Hubbard model over broad regions of the parameter space by several approximate methods, such as Hartree-Fock [27], slave boson mean-field theory [28], expansion in the hole density [29], moderate coupling fRG [30], and dynamical mean-field theory [31, 32]. In our theory the mean-field order applies only to the chargons, while the physical electrons are subject to order parameter fluctuations.

III. COMPUTATION OF PARAMETERS

In this section, we describe how we evaluate the chargon integral in Eq. (11) to compute the magnetic order parameter and the stiffness matrix $\mathcal{J}_{\mu\nu}$. The advantage of the way we formulated our theory in Sec. II is that it allows arbitrary approximations on the chargon action. One can employ various techniques to obtain the order parameter and the spin stiffnesses in the magnetically ordered phase. We use a renormalized mean-field (MF) approach with effective interactions obtained from a functional renormalization group (fRG) flow. In the following we briefly describe our approximation of the (exact) fRG flow, and we refer to Refs. [19, 33, 34] for the fRG, and to Refs. [16, 30, 35, 36] for the fRG+MF method.

A. Symmetric regime

We evaluate the chargon functional integral by using an fRG flow equation [19, 33, 34], choosing the temperature T as flow parameter [37]. Temperature can be used as a flow parameter after rescaling the chargon fields as $\psi_j \rightarrow T^{\frac{3}{2}} \psi_j$, and defining a rescaled bare Green's function, $G_0^T(\mathbf{k}, i\nu_n) = T^{\frac{1}{2}} / (i\nu_n - \epsilon_{\mathbf{k}} + \mu)$, where $\nu_n = (2n + 1)\pi T$ is the fermionic Matsubara frequency, and $\epsilon_{\mathbf{k}}$ is the Fourier transform of the hopping matrix in (1).

We approximate the exact fRG flow by a second order (one-loop) flow of the two-particle vertex V^T , discarding self-energy feedback and contributions from the three-particle vertex [19]. In a $SU(2)$ invariant system the two-particle vertex has the spin structure

$$V_{\sigma_1 \sigma_2 \sigma_3 \sigma_4}^T(k_1, k_2, k_3, k_4) = V^T(k_1, k_2, k_3, k_4) \delta_{\sigma_1 \sigma_3} \delta_{\sigma_2 \sigma_4} - V^T(k_2, k_1, k_3, k_4) \delta_{\sigma_1 \sigma_4} \delta_{\sigma_2 \sigma_3},$$

where $k_\alpha = (\mathbf{k}_\alpha, i\nu_{\alpha n})$ are combined momentum and frequency variables. Translation invariance imposes momentum conservation so that $k_1 + k_2 = k_3 + k_4$. We perform a static approximation, that is, we neglect the frequency dependency of the vertex. To parametrize the momentum dependence, we use the channel decomposition [38–41]

$$\begin{aligned} V^T(\mathbf{k}_1, \mathbf{k}_2, \mathbf{k}_3, \mathbf{k}_4) &= U - \phi_{\frac{\mathbf{k}_1 - \mathbf{k}_2}{2}, \frac{\mathbf{k}_3 - \mathbf{k}_4}{2}}^{p,T}(\mathbf{k}_1 + \mathbf{k}_2) \\ &+ \phi_{\frac{\mathbf{k}_1 + \mathbf{k}_4}{2}, \frac{\mathbf{k}_2 + \mathbf{k}_3}{2}}^{m,T}(\mathbf{k}_2 - \mathbf{k}_3) + \frac{1}{2} \phi_{\frac{\mathbf{k}_1 + \mathbf{k}_3}{2}, \frac{\mathbf{k}_2 + \mathbf{k}_4}{2}}^{m,T}(\mathbf{k}_3 - \mathbf{k}_1) \\ &- \frac{1}{2} \phi_{\frac{\mathbf{k}_1 + \mathbf{k}_3}{2}, \frac{\mathbf{k}_2 + \mathbf{k}_4}{2}}^{c,T}(\mathbf{k}_3 - \mathbf{k}_1), \end{aligned} \quad (25)$$

where the functions $\phi^{p,T}$, $\phi^{m,T}$, and $\phi^{c,T}$ capture fluctuations in the pairing, magnetic, and charge channel, respectively. The dependences of these functions on the linear combination of momenta in the brackets are typically much stronger than those in the subscripts. Hence, we expand the latter dependencies in form factors [38, 42],

keeping only the lowest order s-wave, extended s-wave, p-wave and d-wave contributions.

We run the fRG flow from the initial temperature $T_{\text{ini}} = \infty$, at which $V^{T_{\text{ini}}} = U$, down to a critical temperature T^* at V^T diverges, signaling the onset of spontaneous symmetry breaking (SSB). If the divergence of the vertex is due to $\phi^{m,T}$, the chargons develop some kind of magnetic order.

B. Order parameter

In the magnetic phase, that is, for $T < T^*$, we assume an order parameter of the form $\langle \psi_{\mathbf{k},\uparrow}^* \psi_{\mathbf{k}+\mathbf{Q},\downarrow} \rangle$, which corresponds to Néel antiferromagnetism if $\mathbf{Q} = (\pi, \pi)$, and to spiral order otherwise.

For $T < T^*$ we simplify the flow equations by decoupling the three channels $\phi^{p,T}$, $\phi^{m,T}$, and $\phi^{c,T}$. The flow equations can then be formally integrated, and the formation of an order parameter can be easily taken into account [16]. We focus on magnetic order and ignore the pairing instability to analyze the non-superconducting “normal” state. In the magnetic channel one thus obtains the magnetic gap equation [30]

$$\Delta_{\mathbf{k}} = \int_{\mathbf{k}'} \bar{V}_{\mathbf{k},\mathbf{k}'}^m(\mathbf{Q}) \frac{f(E_{\mathbf{k}'}^-) - f(E_{\mathbf{k}'}^+)}{E_{\mathbf{k}'}^+ - E_{\mathbf{k}'}^-} \Delta_{\mathbf{k}'}, \quad (26)$$

where $f(x) = (e^{x/T} + 1)^{-1}$ is the Fermi function, $\int_{\mathbf{k}}$ is a shorthand notation for $\int \frac{d^2\mathbf{k}}{(2\pi)^2}$, and $E_{\mathbf{k}}^{\pm}$ are the quasiparticle dispersions

$$E_{\mathbf{k}}^{\pm} = \frac{\epsilon_{\mathbf{k}} + \epsilon_{\mathbf{k}+\mathbf{Q}}}{2} \pm \sqrt{\frac{1}{4}(\epsilon_{\mathbf{k}} - \epsilon_{\mathbf{k}+\mathbf{Q}})^2 + \Delta_{\mathbf{k}}^2} - \mu. \quad (27)$$

The effective coupling $\bar{V}_{\mathbf{k},\mathbf{k}'}^m(\mathbf{Q})$ is the particle-hole irreducible part of V^{T^*} in the magnetic channel, which can be obtained by inverting a Bethe-Salpeter equation at the critical scale,

$$V_{\mathbf{k},\mathbf{k}'}^{m,T^*}(\mathbf{q}) = \bar{V}_{\mathbf{k},\mathbf{k}'}^m(\mathbf{q}) - \int_{\mathbf{k}''} \bar{V}_{\mathbf{k},\mathbf{k}''}^m(\mathbf{q}) \Pi_{\mathbf{k}'',\mathbf{k}'}^{T^*}(\mathbf{q}) V_{\mathbf{k}'',\mathbf{k}'}^{m,T^*}(\mathbf{q}), \quad (28)$$

where $V_{\mathbf{k},\mathbf{k}'}^{m,T}(\mathbf{q}) = V^T(\mathbf{k}-\mathbf{q}/2, \mathbf{k}'+\mathbf{q}/2, \mathbf{k}'-\mathbf{q}/2, \mathbf{k}+\mathbf{q}/2)$, and the particle-hole bubble is given by

$$\Pi_{\mathbf{k}}^T(\mathbf{q}) = \sum_{\nu_n} G_0^T(\mathbf{k}-\mathbf{q}/2, i\nu_n) G_0^T(\mathbf{k}+\mathbf{q}/2, i\nu_n). \quad (29)$$

Although $V_{\mathbf{k},\mathbf{k}'}^{m,T^*}(\mathbf{q})$ diverges at certain wave vectors $\mathbf{q} = \mathbf{Q}_c$, the irreducible coupling $\bar{V}_{\mathbf{k},\mathbf{k}'}^m(\mathbf{q})$ is finite for all \mathbf{q} .

The dependence of $\bar{V}_{\mathbf{k},\mathbf{k}'}^m(\mathbf{q})$ on \mathbf{k} and \mathbf{k}' is rather weak and of no qualitative importance. Hence, to simplify the calculations, we discard the \mathbf{k} and \mathbf{k}' dependencies of the effective coupling by taking the momentum average $\bar{V}^m(\mathbf{q}) = \int_{\mathbf{k},\mathbf{k}'} \bar{V}_{\mathbf{k},\mathbf{k}'}^m(\mathbf{q})$. The magnetic gap then becomes

momentum independent, that is, $\Delta_{\mathbf{k}} = \Delta$. While the full vertex $V_{\mathbf{k},\mathbf{k}'}^{m,T}(\mathbf{q})$ depends very strongly on \mathbf{q} , the dependence of its irreducible part $\bar{V}_{\mathbf{k},\mathbf{k}'}^m(\mathbf{q})$ on \mathbf{q} is rather weak. The calculation of the stiffnesses in the subsequent section is considerably simplified approximating $\bar{V}^m(\mathbf{q})$ by a momentum independent effective interaction $U_{\text{eff}}^m = \bar{V}^m(\mathbf{Q}_c)$.

The optimal ordering wave vector \mathbf{Q} is found by minimizing the mean-field free energy of the system

$$F(\mathbf{Q}) = -T \int_{\mathbf{k}} \sum_{\ell=\pm} \ln \left(1 + e^{-E_{\mathbf{k}}^{\ell}(\mathbf{Q})/T} \right) + \frac{\Delta^2}{2U_{\text{eff}}^m} + \mu n, \quad (30)$$

where the chemical potential μ is determined by keeping the density $n = \int_{\mathbf{k}} \sum_{\ell=\pm} f(E_{\mathbf{k}}^{\ell})$ fixed. The optimal wave vectors \mathbf{Q} at temperatures $T < T^*$ generally differ from the wave vectors \mathbf{Q}_c at which $V_{\mathbf{k},\mathbf{k}'}^{T^*}(\mathbf{q})$ diverges.

Eq. (26) has the form of a mean-field gap equation with a renormalized interaction that is reduced compared to the bare Hubbard interaction U by fluctuations in the pairing and charge channels. This reduces the critical doping beyond which magnetic order disappears, compared to the unrealistically large values obtained already for weak bare interactions in pure Hartree-Fock theory (see e.g. Ref. [27]).

C. Spin stiffnesses

The NL σ M parameters, that is, the spin stiffnesses $\mathcal{J}_{\mu\nu}^{ab}$, are obtained by evaluating Eq. (15). These expressions can be viewed as the response of the chargon system to an external SU(2) gauge field in the low energy and long wavelength limit, and they are equivalent to the stiffnesses defined by an expansion of the inverse susceptibilities to quadratic order in momentum and frequency around the Goldstone poles [17, 43]. The following evaluation is obtained as a simple generalization of the RPA formula derived in Ref. [17] to a renormalized RPA with effective interactions U_{eff}^m and U_{eff}^c . Since in the magnetic state the translational symmetry is broken, the Fourier transforms of the response functions depend on two distinct momenta \mathbf{q} and \mathbf{q}' , where \mathbf{q}' can assume the values \mathbf{q} , $\mathbf{q} \pm \mathbf{Q}$, and $\mathbf{q} \pm 2\mathbf{Q}$. However, to compute $\mathcal{J}_{\mu\nu}^{ab}$, we only need to deal with the limit $\mathbf{q}, \mathbf{q}' \rightarrow \mathbf{0}$.

The temporal components of the stiffness matrix, that is, \mathcal{J}_{00}^{ab} , are given by the uniform spin susceptibility in the dynamical limit [17]

$$\mathcal{J}_{00}^{ab} = -\chi_{\text{dyn}}^{ab} = -\lim_{\omega \rightarrow 0} \chi^{ab}(\mathbf{0}, \mathbf{0}, \omega), \quad (31)$$

where $\chi^{ab}(\mathbf{q}, \mathbf{q}', \omega)$ is the Fourier transform of

$$\chi_{jl}^{ab}(\tau) = \frac{1}{4} \langle (\psi_j^*(\tau) \sigma^a \psi_j(\tau)) (\psi_l^*(0) \sigma^b \psi_l(0)) \rangle_c. \quad (32)$$

Note that, in a metallic system, the static uniform susceptibility obtained from $\mathbf{q}, \mathbf{q}' \rightarrow \mathbf{0}$ after setting $\omega = 0$ differs from the quantity defined in Eq. (31).

The spin susceptibility can be most conveniently computed in a rotating spin frame defined by the transformation [43, 44]

$$\tilde{\psi}_j = e^{-i\frac{\mathbf{Q}}{2} \cdot \mathbf{r}_j} e^{i\sigma^3 \frac{\mathbf{Q}}{2} \cdot \mathbf{r}_j} \psi_j, \quad \tilde{\psi}_j^* = \psi_j^* e^{-i\sigma^3 \frac{\mathbf{Q}}{2} \cdot \mathbf{r}_j} e^{i\frac{\mathbf{Q}}{2} \cdot \mathbf{r}_j}, \quad (33)$$

since in the rotated frame the magnetically ordered system appears translation invariant. Hence, the rotated susceptibility is diagonal in momentum space and can therefore be written as $\tilde{\chi}^{ab}(\mathbf{q}, \omega)$, with a single momentum variable \mathbf{q} .

Consistently with the mean-field theory for the magnetic order parameter, we compute the susceptibilities in the magnetic state via a random phase approximation (RPA) with renormalized interactions as obtained from the fRG. In a spiral state with a generic wave vector \mathbf{Q} , the spin susceptibility is coupled to the charge susceptibility [44]. Hence, we extend the definition of the spin susceptibility in Eq. (32) to a combined charge-spin susceptibility by including the value 0 for the indices a and b , in addition to the values 1, 2, 3, and defining σ^0 as the two-dimensional unit matrix. The prefactor $\frac{1}{4}$ in Eq. (32) implies that χ^{00} is actually a quarter of the conventional charge susceptibility.

In RPA, the rotated susceptibility $\tilde{\chi}$ can be written as

$$\tilde{\chi}^{ab}(q) = \tilde{\chi}_0^{ab}(q) + \sum_{a', b'=0}^3 \tilde{\chi}_0^{aa'}(q) \tilde{\Gamma}^{a'b'}(q) \tilde{\chi}_0^{b'b}(q), \quad (34)$$

where $q = (\mathbf{q}, \omega)$, and $\tilde{\Gamma}^{ab}(q)$ is the RPA effective interaction in the rotated spin frame. The ‘‘bare’’ susceptibility $\tilde{\chi}_0^{ab}(q)$ is given by the particle-hole bubble [43]

$$\tilde{\chi}_0^{ab}(\mathbf{q}, \omega) = -\frac{1}{4} \int_{\mathbf{k}} T \sum_{\nu_n} \text{Tr} [\sigma^a \tilde{\mathcal{G}}(\mathbf{k} + \mathbf{q}, i\nu_n + \omega + i0^+) \times \sigma^b \tilde{\mathcal{G}}(\mathbf{k}, i\nu_n)], \quad (35)$$

with $\tilde{\mathcal{G}}(\mathbf{k}, i\nu_n)$ the mean-field chargin Green’s function in the rotated basis

$$\tilde{\mathcal{G}}(\mathbf{k}, i\nu_n) = \begin{pmatrix} i\nu_n - \epsilon_{\mathbf{k}} + \mu & -\Delta \\ -\Delta & i\nu_n - \epsilon_{\mathbf{k}+\mathbf{Q}} + \mu \end{pmatrix}^{-1}. \quad (36)$$

The RPA effective interaction is obtained from a ladder sum, leading to the linear matrix equation

$$\tilde{\Gamma}^{ab}(q) = \tilde{\Gamma}_0^{ab}(\mathbf{q}) + \sum_{a', b'=0}^3 \tilde{\Gamma}_0^{aa'}(\mathbf{q}) \tilde{\chi}_0^{a'b'}(q) \tilde{\Gamma}^{b'b}(q), \quad (37)$$

where

$$\tilde{\Gamma}_0^{ab}(\mathbf{q}) = \Gamma_0^{ab}(\mathbf{q}) = 2 \text{diag} [-U_{\text{eff}}^c(\mathbf{q}), U_{\text{eff}}^m, U_{\text{eff}}^m, U_{\text{eff}}^m]. \quad (38)$$

The effective charge interaction is given by $U_{\text{eff}}^c(\mathbf{q}) = \int_{\mathbf{k}, \mathbf{k}'} \bar{V}_{\mathbf{k}, \mathbf{k}'}^c(\mathbf{q})$, where the irreducible coupling $\bar{V}_{\mathbf{k}, \mathbf{k}'}^c(\mathbf{q})$ is obtained by inverting a Bethe-Salpeter equation similar

to Eq. (28),

$$V_{\mathbf{k}, \mathbf{k}'}^{c, T^*}(\mathbf{q}) = \bar{V}_{\mathbf{k}, \mathbf{k}'}^c(\mathbf{q}) + \int_{\mathbf{k}''} \bar{V}_{\mathbf{k}, \mathbf{k}''}^c(\mathbf{q}) \Pi_{\mathbf{k}''}^{T^*}(\mathbf{q}) V_{\mathbf{k}'', \mathbf{k}'}^{c, T^*}(\mathbf{q}), \quad (39)$$

with

$$V_{\mathbf{k}, \mathbf{k}'}^{c, T}(\mathbf{q}) = 2V^T(\mathbf{k} - \mathbf{q}/2, \mathbf{k}' + \mathbf{q}/2, \mathbf{k} + \mathbf{q}/2, \mathbf{k}' - \mathbf{q}/2) - V^T(\mathbf{k} - \mathbf{q}/2, \mathbf{k}' + \mathbf{q}/2, \mathbf{k}' - \mathbf{q}/2, \mathbf{k} + \mathbf{q}/2).$$

Here we keep the dependence on \mathbf{q} since it does not complicate the calculations. The off-diagonal ($a \neq b$) elements of $\chi^{ab}(\mathbf{0}, \mathbf{0}, \omega)$ with $a, b = 1, 2, 3$ vanish for $\omega \rightarrow 0$ both in the spiral and in the Néel state, so that we need to deal only with the diagonal spin susceptibility components $\chi^{aa}(\mathbf{q}, \mathbf{q}, \omega)$.

In a spiral state with $\mathbf{Q} \neq (\pi, \pi)$, the diagonal (both in momentum and spin indices) spin susceptibility components are related to the susceptibility components in the rotated basis as [43]

$$\begin{aligned} \chi^{11}(\mathbf{q}, \mathbf{q}, \omega) &= \chi^{22}(\mathbf{q}, \mathbf{q}, \omega) \\ &= \frac{1}{4} \sum_{s=\pm} [\tilde{\chi}^{11}(q + sQ) + \tilde{\chi}^{22}(q + sQ)] \\ &\quad + 2i\tilde{\chi}^{12}(q + Q) + 2i\tilde{\chi}^{21}(q - Q), \quad (40a) \end{aligned}$$

$$\chi^{33}(\mathbf{q}, \mathbf{q}, \omega) = \tilde{\chi}^{33}(q), \quad (40b)$$

where $Q = (\mathbf{Q}, 0)$. The momentum diagonal components of $\chi^{11}(\mathbf{q}, \mathbf{q}', \omega)$ and $\chi^{22}(\mathbf{q}, \mathbf{q}', \omega)$ are equal, and the limit $\omega \rightarrow 0$ in (31) is nonzero for all diagonal components, yielding

$$\mathcal{J}_{00} = \begin{pmatrix} -Z^\perp & 0 & 0 \\ 0 & -Z^\perp & 0 \\ 0 & 0 & -Z^\square \end{pmatrix}, \quad (41)$$

with $Z^\perp = \chi^{22}(\mathbf{0}, \mathbf{0}, \omega \rightarrow 0)$ and $Z^\square = \chi^{33}(\mathbf{0}, \mathbf{0}, \omega \rightarrow 0)$. The quantities Z^\square and Z^\perp parametrize the low frequency dependence of the in-plane and out-of-plane spin susceptibility, respectively, near the Goldstone poles [17, 43].

In the limits $\omega \rightarrow 0$ and $\mathbf{q} \rightarrow \mathbf{0}$ or \mathbf{Q} , several off-diagonal matrix elements of the RPA effective interaction $\tilde{\Gamma}^{ab}(\mathbf{q}, \omega)$ vanish [43]. The expressions for Z^a can therefore be simplified to [17]

$$Z^\square = \frac{\tilde{\chi}_0^{33}(\mathbf{0}, \omega \rightarrow 0)}{1 - 2U_{\text{eff}}^m \tilde{\chi}_0^{33}(\mathbf{0}, \omega \rightarrow 0)}, \quad (42)$$

and

$$\begin{aligned} Z^\perp &= 2\tilde{\chi}_0^{-+}(\mathbf{Q}, 0) \\ &\quad + 2 \sum_{a,b=0,1,2} \tilde{\chi}_0^{-a}(\mathbf{Q}, 0) \tilde{\Gamma}^{ab}(\mathbf{Q}, 0) \tilde{\chi}_0^{b+}(\mathbf{Q}, 0), \quad (43) \end{aligned}$$

where superscripts $+$ and $-$ attached to $\tilde{\chi}_0$ indicate that the susceptibilities are formed with the ladder operators $S^\pm = \frac{1}{2}(S^1 \pm S^2)$.

In the Néel state, terms which contribute to $\chi^{11}(\mathbf{q}, \mathbf{q}', \omega)$ and $\chi^{22}(\mathbf{q}, \mathbf{q}', \omega)$ with $\mathbf{q}' = \mathbf{q} \pm 2\mathbf{Q}$ for $\mathbf{Q} \neq (\pi, \pi)$, contribute to the momentum diagonal susceptibilities since $2\mathbf{Q} \equiv \mathbf{0}$ for $\mathbf{Q} = (\pi, \pi)$. The transformation of the susceptibilities from the rotated to the unrotated basis then reads [43]

$$\chi^{11}(\mathbf{q}, \mathbf{q}, \omega) = \tilde{\chi}^{11}(q + Q), \quad (44a)$$

$$\chi^{22}(\mathbf{q}, \mathbf{q}, \omega) = \tilde{\chi}^{22}(q + Q), \quad (44b)$$

$$\chi^{33}(\mathbf{q}, \mathbf{q}, \omega) = \tilde{\chi}^{33}(q). \quad (44c)$$

Since $\tilde{\chi}^{11}(\mathbf{Q}, \omega) = 0$ and $\tilde{\chi}^{22}(q + Q) = \tilde{\chi}^{33}(q)$ for $\mathbf{Q} = (\pi, \pi)$, we obtain

$$\mathcal{J}_{00} = \begin{pmatrix} 0 & 0 & 0 \\ 0 & -Z & 0 \\ 0 & 0 & -Z \end{pmatrix}, \quad (45)$$

with $Z = \chi^{22}(\mathbf{0}, \mathbf{0}, \omega \rightarrow 0)$ in the Néel state, which can be evaluated by the same expression as the one for Z^\square in Eq. (42).

The spatial components of the stiffness matrix $\mathcal{J}_{\alpha\beta}^{ab}$ with $\alpha, \beta = 1, 2$ are obtained from the spatial components of the uniform gauge field kernel $\mathcal{K}_{\alpha\beta}^{ab}$ in the *static* limit [17]

$$\mathcal{J}_{\alpha\beta}^{ab} = - \lim_{\mathbf{q} \rightarrow \mathbf{0}} \mathcal{K}_{\alpha\beta}^{ab}(\mathbf{q}, \mathbf{q}, 0), \quad (46)$$

where $\mathcal{K}_{\alpha\beta}^{ab}(\mathbf{q}, \mathbf{q}', \omega) = \mathcal{K}_{\alpha\beta}^{p,ab}(\mathbf{q}, \mathbf{q}', \omega) + \delta_{ab} \mathcal{K}_{\alpha\beta}^d$ is the Fourier transform of

$$\mathcal{K}_{\alpha\beta, jl}^{ab}(\tau) = \mathcal{K}_{\alpha\beta, jl}^{p,ab}(\tau) + \mathcal{K}_{\alpha\beta}^d \delta_{ab} \delta_{jl} \delta(\tau), \quad (47)$$

with the paramagnetic and diamagnetic contributions (cf. Eq. (15))

$$\begin{aligned} \mathcal{K}_{\alpha\beta, jl}^{p,ab}(\tau) &= \frac{1}{4} \sum_{j', l'} \gamma_\alpha^{(1)}(j, j') \gamma_\beta^{(1)}(l, l') \\ &\times \langle (\psi_j^*(\tau) \sigma^a \psi_{j'}(\tau)) (\psi_l^*(0) \sigma^b \psi_{l'}(0)) \rangle_c, \end{aligned} \quad (48)$$

$$\mathcal{K}_{\alpha\beta}^d = -\frac{1}{4} \sum_{j'} \gamma_{\alpha\beta}^{(2)}(j, j') \langle \psi_j^*(0) \psi_{j'}(0) \rangle, \quad (49)$$

respectively. The diamagnetic contribution is translation invariant (in a spiral or Néel state). Fourier transforming, and evaluating the expectation value in Eq. (48) by the renormalized RPA, the paramagnetic part of the spin stiffness can be written as

$$\begin{aligned} \mathcal{J}_{\alpha\beta}^{p,ab} &= - \lim_{\mathbf{q} \rightarrow \mathbf{0}} \left[\mathcal{K}_{0, \alpha\beta}^{p,ab}(\mathbf{q}, \mathbf{q}, 0) \right. \\ &+ \sum_{a', b'=0}^3 \int_{\mathbf{q}', \mathbf{q}''} \mathcal{K}_{0, \alpha 0}^{p, a a'}(\mathbf{q}, \mathbf{q}', 0) \\ &\left. \times \Gamma^{a' b'}(\mathbf{q}', \mathbf{q}'', 0) \mathcal{K}_{0, 0 \beta}^{p, b' b}(\mathbf{q}'', \mathbf{q}, 0) \right], \end{aligned} \quad (50)$$

where $\Gamma^{ab}(\mathbf{q}, \mathbf{q}', \omega)$ is the RPA effective interaction (37) in the original (non-rotated) spin basis. The bare paramagnetic response kernel is given by

$$\begin{aligned} \mathcal{K}_{0, \mu\nu}^{p, ab}(\mathbf{q}, \mathbf{q}', 0) &= -\frac{1}{4} \int_{\mathbf{k}, \mathbf{k}'} T \sum_{\nu_n} \gamma_\mu^{(1)}(\mathbf{k} + \mathbf{q}) \gamma_\nu^{(1)}(\mathbf{k}') \\ &\times \text{Tr} [\sigma^a \mathcal{G}(\mathbf{k} + \mathbf{q}, \mathbf{k}' + \mathbf{q}', i\nu_n) \sigma^b \mathcal{G}(\mathbf{k}', \mathbf{k}, i\nu_n)], \end{aligned} \quad (51)$$

where $\gamma^{(1)}(\mathbf{k}) = (1, \partial_{k_x} \epsilon_{\mathbf{k}}, \partial_{k_y} \epsilon_{\mathbf{k}})$ is the Fourier transform of $\gamma^{(1)}(j, j')$ in Eq. (16a). The chargin Green's function in the original spin basis reads

$$\mathcal{G}(\mathbf{k}, \mathbf{k}', i\nu_n) = \begin{pmatrix} G_{+\mathbf{Q}}(k) \delta_{\mathbf{k}, \mathbf{k}'} & F_{+\mathbf{Q}}(k) \delta_{\mathbf{k} + \mathbf{Q}, \mathbf{k}'} \\ F_{-\mathbf{Q}}(k) \delta_{\mathbf{k} - \mathbf{Q}, \mathbf{k}'} & G_{-\mathbf{Q}}(k) \delta_{\mathbf{k}, \mathbf{k}'} \end{pmatrix}, \quad (52)$$

with

$$G_{\pm\mathbf{Q}}(k) = \frac{i\nu_n - \epsilon_{\mathbf{k} \pm \mathbf{Q}} + \mu}{(i\nu_n - \epsilon_{\mathbf{k}} + \mu)(i\nu_n - \epsilon_{\mathbf{k} \pm \mathbf{Q}} + \mu) - \Delta^2}, \quad (53a)$$

$$F_{\pm\mathbf{Q}}(k) = \frac{\Delta}{(i\nu_n - \epsilon_{\mathbf{k}} + \mu)(i\nu_n - \epsilon_{\mathbf{k} \pm \mathbf{Q}} + \mu) - \Delta^2}. \quad (53b)$$

The diamagnetic part of the spin stiffness can be obtained from the Green's function as

$$\mathcal{J}_{\alpha\beta}^{d, ab} = \frac{\delta_{ab}}{4} \int_{\mathbf{k}, \mathbf{k}'} T \sum_{\nu_n} \gamma_{\alpha\beta}^{(2)}(\mathbf{k}) \text{tr} [\mathcal{G}(\mathbf{k}, \mathbf{k}', i\nu_n)] \quad (54)$$

where $\gamma_{\alpha\beta}^{(2)}(\mathbf{k}) = \partial_{k_\alpha} \partial_{k_\beta} \epsilon_{\mathbf{k}}$ is the Fourier transform of the second order current vertex $\gamma_{\alpha\beta}^{(2)}(j, j')$ in Eq. (16b). The various contributions to the response kernel are represented diagrammatically in Fig. 1.

The off-diagonal ($a \neq b$) components of $\mathcal{K}_{\alpha\beta}^{ab}(\mathbf{q}, \mathbf{q}, 0)$ vanish for $\mathbf{q} \rightarrow \mathbf{0}$ in the spiral and in the Néel state, so that we need to consider only the diagonal components. For $a = b = 1, 2$ only the first (bare) term in Eq. (50) contributes to the stiffness [17]. In a spiral state with $\mathbf{Q} \neq (\pi, \pi)$, one thus obtains the out-of-plane stiffness as

$$J_{\alpha\beta}^\perp = \mathcal{J}_{\alpha\beta}^{11} = \mathcal{J}_{\alpha\beta}^{22} = - \lim_{\mathbf{q} \rightarrow \mathbf{0}} \mathcal{K}_{0, \alpha\beta}^{p, 22}(\mathbf{q}, \mathbf{q}, 0) - \mathcal{K}_{\alpha\beta}^d. \quad (55)$$

For $a = b = 3$, there are non vanishing components of the kernel that mix temporal and spatial indices, namely

$$\mathcal{K}_{0, \alpha 0}^{p, 30}(\mathbf{q}, \mathbf{q}', 0) = \mathcal{K}_{0, 0\alpha}^{p, 03}(\mathbf{q}, \mathbf{q}', 0) = \mathcal{K}_{0, \alpha 0}^{p, 30}(\mathbf{q}, 0) \delta_{\mathbf{q}, \mathbf{q}'}, \quad (56a)$$

$$\begin{aligned} \mathcal{K}_{0, \alpha 0}^{p, 31}(\mathbf{q}, \mathbf{q}', 0) &= \mathcal{K}_{0, 0\alpha}^{p, 13}(\mathbf{q}, \mathbf{q}', 0) \\ &= \mathcal{K}_{0, \alpha 0}^{p, 31}(\mathbf{q}, 0) \frac{\delta_{\mathbf{q} + \mathbf{Q}, \mathbf{q}'} + \delta_{\mathbf{q} - \mathbf{Q}, \mathbf{q}'}}{2}, \end{aligned} \quad (56b)$$

$$\begin{aligned} \mathcal{K}_{0, \alpha 0}^{p, 32}(\mathbf{q}, \mathbf{q}', 0) &= \mathcal{K}_{0, 0\alpha}^{p, 23}(\mathbf{q}, \mathbf{q}', 0) \\ &= \mathcal{K}_{0, \alpha 0}^{p, 32}(\mathbf{q}, 0) \frac{\delta_{\mathbf{q} + \mathbf{Q}, \mathbf{q}'} - \delta_{\mathbf{q} - \mathbf{Q}, \mathbf{q}'}}{2i}. \end{aligned} \quad (56c)$$

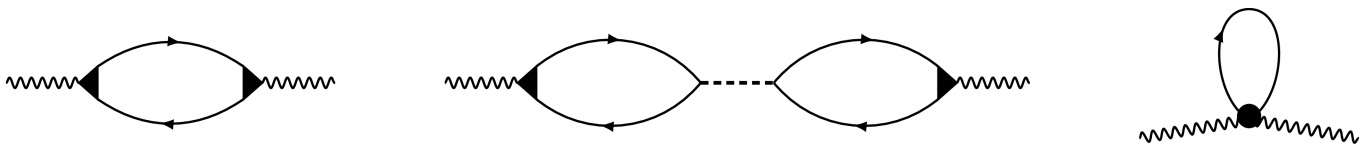


Figure 1. Diagrams contributing to the spin stiffness. The black triangles and circles represent the first and second order current vertices $\gamma_{\alpha}^{(1)}(\mathbf{k})$ and $\gamma_{\alpha\beta}^{(2)}(\mathbf{k})$, respectively, while the dashed line represents the effective interaction $\Gamma^{ab}(\mathbf{q}, \mathbf{q}', \omega)$.

Using $\mathcal{K}_{0,\alpha 0}^{\text{p},31}(\mathbf{q} \rightarrow \mathbf{0}, 0) = \mathcal{K}_{0,\alpha 0}^{\text{p},32}(\mathbf{q} \rightarrow \mathbf{0}, 0)$, one thus obtains the in-plane stiffness in the form [17]

$$J_{\alpha\beta}^{\square} = \mathcal{J}_{\alpha\beta}^{33} = - \lim_{\mathbf{q} \rightarrow 0} \mathcal{K}_{0,\alpha\beta}^{\text{p},33}(\mathbf{q}, \mathbf{q}, 0) - \mathcal{K}_{\alpha\beta}^{\text{d}} - \lim_{\mathbf{q} \rightarrow 0} \sum_{a,b=0,1} \mathcal{K}_{0,\alpha 0}^{\text{p},3a}(\mathbf{q}, 0) \tilde{\Gamma}^{ab}(\mathbf{q}, 0) \mathcal{K}_{0,\beta 0}^{\text{p},3b}(\mathbf{q}, 0), \quad (57)$$

where $\tilde{\Gamma}^{ab}(q)$ is the effective interaction in the spin rotated basis, see Eq. (37).

In the Néel state one finds, in close analogy to the temporal components \mathcal{J}_{00}^{ab} of the stiffness matrix, $\mathcal{J}_{\alpha\beta}^{11} = 0$ and $\mathcal{J}_{\alpha\beta}^{22} = \mathcal{J}_{\alpha\beta}^{33} = J\delta_{\alpha\beta}$, which can be most easily computed from the right hand side of Eq. (55).

In our low energy theory of the spinons we have ignored possible imaginary contributions from Landau damping of the Goldstone modes. In a Néel state, they are of the same order in the gradient expansion as the (real) temporal and spatial stiffness terms [45]. The same is true for the Landau damping of the in-plane mode in a spiral state, but the damping of the out-of-plane mode is of higher order [43]. Moreover, it requires the existence of hot spots (connected by \mathbf{Q}) of the reconstructed Fermi surface. In our large N evaluation of the NL σ M, the in-plane modes of the spiral state do not contribute. Hence, for the spiral state, Landau damping is irrelevant for our theory, while in the Néel state their might be a quantitative (not qualitative) modification of our results.

We conclude this section by comparing our theory to the SU(2) gauge theory of the half-filled Hubbard model derived by Borejsza and Dupuis [14]. They used the same fractionalization of the electron in chargons and spinons, and the chargon order was treated in (plain) mean-field theory. Our expressions for the spin stiffnesses agree with theirs (at half-filling) if we replace our renormalized interaction U_{eff}^m by the bare Hubbard interaction U , although their derivation differs from ours. Following earlier work by Haldane [20, 21] for the Heisenberg model, Borejsza and Dupuis obtained their expressions for the spin stiffnesses by splitting the spinon into a “Néel field” and a “canting field” describing ferromagnetic fluctuations. Integrating out the fermions and the canting field they obtained a NL σ M for the Néel field, where the stiffnesses are given by the RPA. We obtain the same expressions (with a renormalized coupling) more directly from the RPA evaluation of the gauge field response, without introducing the canting field.

IV. EVALUATION OF SIGMA MODEL

To solve the NL σ M, we resort to a saddle point approximation in the CP^{N-1} representation, which is exact in the large N limit [46, 47].

A. CP^1 representation

The matrix \mathcal{R} can be expressed as a triad of orthonormal unit vectors:

$$\mathcal{R} = (\hat{\Omega}_1, \hat{\Omega}_2, \hat{\Omega}_3), \quad (58)$$

where $\hat{\Omega}_i \cdot \hat{\Omega}_j = \delta_{ij}$. We represent these vectors in terms of two complex Schwinger bosons z_{\uparrow} and z_{\downarrow} [45]

$$\hat{\Omega}_- = z(i\sigma^2 \vec{\sigma})z, \quad (59a)$$

$$\hat{\Omega}_+ = z^*(i\sigma^2 \vec{\sigma})^\dagger z^*, \quad (59b)$$

$$\hat{\Omega}_3 = z^* \vec{\sigma} z, \quad (59c)$$

with $z = (z_{\uparrow}, z_{\downarrow})$ and $\hat{\Omega}_{\pm} = \hat{\Omega}_1 \mp i\hat{\Omega}_2$. The Schwinger bosons obey the nonlinear constraint

$$z_{\uparrow}^* z_{\uparrow} + z_{\downarrow}^* z_{\downarrow} = 1. \quad (60)$$

The parametrization (59) is equivalent to

$$R = \begin{pmatrix} z_{\uparrow} & -z_{\downarrow}^* \\ z_{\downarrow} & z_{\uparrow}^* \end{pmatrix}. \quad (61)$$

Inserting the expressions (58) and (59) into Eq. (18) and assuming a stiffness matrix $\mathcal{J}_{\mu\nu}$ of the form (23), we obtain the CP^1 action for fluctuating spiral order

$$\mathcal{S}_{\text{CP}^1}[z, z^*] = \int_{\mathcal{T}} dx \left[2J_{\mu\nu}^{\perp} (\partial_{\mu} z^*) (\partial_{\nu} z) - 2(J_{\mu\nu}^{\perp} - J_{\mu\nu}^{\square}) j_{\mu} j_{\nu} \right], \quad (62)$$

with sum convention for repeated greek indices and the current operator

$$j_{\mu} = \frac{i}{2} [z^* (\partial_{\mu} z) - (\partial_{\mu} z^*) z]. \quad (63)$$

For the Néel case, the CP^1 action is given by the same expression with $J_{\mu\nu}^{\square} = 0$. We recall that $x = (\tau, \mathbf{r})$ comprises the imaginary time and space variables, and $\mathcal{T} = [0, \beta] \times \mathbb{R}^2$.

B. Large N expansion

The current-current interaction in Eq. (62) can be decoupled by a Hubbard-Stratonovich transformation, introducing a U(1) gauge field \mathcal{A}_μ , and implementing the constraint (60) by means of a Lagrange multiplier λ . The resulting form of the action describes the so-called massive CP¹ model [48]

$$\mathcal{S}_{\text{CP}^1}[z, z^*, \mathcal{A}_\mu, \lambda] = \int_{\mathcal{T}} dx \left[2J_{\mu\nu}^\perp (D_\mu z)^* (D_\nu z) + \frac{1}{2} M_{\mu\nu} \mathcal{A}_\mu \mathcal{A}_\nu + i\lambda(z^* z - 1) \right], \quad (64)$$

where $D_\mu = \partial_\mu - i\mathcal{A}_\mu$ is the covariant derivative. The numbers $M_{\mu\nu}$ are the matrix elements of the mass tensor of the U(1) gauge field,

$$M = 4[1 - J^\square (J^\perp)^{-1}]^{-1} J^\square, \quad (65)$$

where J^\square and J^\perp are the stiffness tensors built from the matrix elements $J_{\mu\nu}^\square$ and $J_{\mu\nu}^\perp$, respectively.

To perform a large N expansion, we extend the two-component field $z = (z_\uparrow, z_\downarrow)$ to an N -component field $z = (z_1, \dots, z_N)$, and rescale it by a factor $\sqrt{N/2}$ so that it now satisfies the constraint

$$z^* z = \sum_{\alpha=1}^N z_\alpha^* z_\alpha = \frac{N}{2}. \quad (66)$$

To obtain a nontrivial limit $N \rightarrow \infty$, we rescale the stiffnesses $J_{\mu\nu}^\perp$ and $J_{\mu\nu}^\square$ by a factor $2/N$, yielding the action

$$\mathcal{S}_{\text{CP}^{N-1}}[z, z^*, \mathcal{A}_\mu, \lambda] = \int_{\mathcal{T}} dx \left[2J_{\mu\nu}^\perp (D_\mu z)^* (D_\nu z) + \frac{N}{4} M_{\mu\nu} \mathcal{A}_\mu \mathcal{A}_\nu + i\lambda \left(z^* z - \frac{N}{2} \right) \right]. \quad (67)$$

This action describes the massive CP ^{$N-1$} model [49], which in $d > 2$ dimensions displays two distinct critical points [47, 48, 50]. The first one belongs to the pure CP ^{$N-1$} class, where $M_{\mu\nu} \rightarrow 0$ ($J_{\mu\nu}^\square = 0$), which applies, for example, in the case of Néel ordering of the chargons, and the U(1) gauge invariance is preserved. The second is in the O(2N) class, where $M_{\mu\nu} \rightarrow \infty$ ($J_{\mu\nu}^\perp = J_{\mu\nu}^\square$) and the gauge field does not propagate. At the leading order in N^{-1} , the saddle point equations are the same for both fixed points, so that we can ignore this distinction in the following.

At finite temperatures $T > 0$ the non-linear sigma model does not allow for any long-range magnetic order, in agreement with the Mermin-Wagner theorem. The spin correlations decay exponentially and the spin excitations are bounded from below by a spin gap $m_s = \sqrt{i\langle \lambda \rangle} / Z^\perp$. In the large N limit, the spin gap m_s is related to the spin stiffness by the following equation (see Appendix C for a derivation)

$$\frac{1}{4\pi J} \int_0^{c_s \Lambda_{\text{uv}}} \frac{\epsilon d\epsilon}{\sqrt{\epsilon^2 + m_s^2}} \coth \left(\frac{\sqrt{\epsilon^2 + m_s^2}}{2T} \right) = 1, \quad (68)$$

where Λ_{uv} is an ultraviolet momentum cutoff. The constant J is an ‘‘average’’ spin stiffness given by

$$J = \sqrt{\det \begin{pmatrix} J_{xx}^\perp & J_{xy}^\perp \\ J_{yx}^\perp & J_{yy}^\perp \end{pmatrix}}, \quad (69)$$

and $c_s = \sqrt{J/Z^\perp}$ is the corresponding average spin wave velocity. In Sec. IV C, we shall discuss how to choose the value of Λ_{uv} . For $m_s \ll c_s \Lambda_{\text{uv}}$, and $T \ll c_s \Lambda_{\text{uv}}$, the magnetic correlation length $\xi_s = \frac{1}{2} c_s / m_s$, behaves as

$$\xi_s = \frac{c_s}{4T \sinh^{-1} \left[\frac{1}{2} e^{-\frac{2\pi}{T}(J-J_c)} \right]}, \quad (70)$$

with the critical stiffness

$$J_c = \frac{c_s \Lambda_{\text{uv}}}{4\pi}. \quad (71)$$

The correlation length is finite at each $T > 0$. For $J > J_c$, ξ_s diverges exponentially for $T \rightarrow 0$, while for $J < J_c$ it remains finite in the zero temperature limit.

At $T = 0$, the bosons may condense and the saddle point condition yields

$$n_0 + \frac{1}{4\pi J} \int_0^{c_s \Lambda_{\text{uv}}} \frac{\epsilon d\epsilon}{\sqrt{\epsilon^2 + m_s^2}} = 1, \quad (72)$$

where $n_0 = |z_1|^2$ is the fraction of condensed bosons. Eq. (72) can be easily solved, yielding (if $m_s \ll \Lambda_{\text{uv}}$)

$$\begin{cases} m_s = 0 \\ n_0 = 1 - \frac{J_c}{J} \end{cases} \quad \text{for } J > J_c, \quad (73a)$$

$$\begin{cases} n_0 = 0 \\ m_s = 2\pi J \left[(J_c/J)^2 - 1 \right] \end{cases} \quad \text{for } J < J_c. \quad (73b)$$

The Mermin-Wagner theorem is thus respected already in the saddle-point approximation to the CP ^{$N-1$} representation of the nonlinear sigma model, that is, there is no long-range order at $T > 0$. In the ground state, long-range order (corresponding to a z boson condensation) is obtained for a sufficiently large spin stiffness, while for $J < J_c$ magnetic order is destroyed by quantum fluctuations even at $T = 0$, giving rise to a paramagnetic state with a spin gap.

C. Choice of ultraviolet cutoff

The impact of spin fluctuations described by the non-linear sigma model depends strongly on the ultraviolet cutoff Λ_{uv} . In particular, the critical stiffness J_c separating a ground state with magnetic long-range order from a disordered ground state is directly proportional to Λ_{uv} . The need for a regularization of the theory by an ultraviolet cutoff is a consequence of the gradient expansion. While the expansion coefficients (the stiffnesses)

are determined by the microscopic model, there is no systematic way of computing Λ_{uv} .

A pragmatic choice for the cutoff is given by the ansatz

$$\Lambda_{uv} = C/\xi_A, \quad (74)$$

where C is a dimensionless number, and ξ_A is the magnetic coherence length, which is the characteristic length scale of spin amplitude correlations. This choice may be motivated by the observation that local moments with a well defined spin amplitude are not defined at length scales below ξ_A [14]. The constant C can be fixed by matching results from the nonlinear sigma model to results from a microscopic calculation in a suitable special case (see below).

The coherence length ξ_A can be obtained from the connected spin amplitude correlation function $\chi_A(\mathbf{r}_j, \mathbf{r}_{j'}) = \langle (\hat{n}_j \cdot \vec{S}_j^\psi)(\hat{n}_{j'} \cdot \vec{S}_{j'}^\psi) \rangle_c$, where $\hat{n}_j = \langle \vec{S}_j^\psi \rangle / |\langle \vec{S}_j^\psi \rangle|$. At long distances between \mathbf{r}_j and $\mathbf{r}_{j'}$ this function decays exponentially with an exponential dependence e^{-r/ξ_A} of the distance r . Fourier transforming and using the rotated spin frame introduced in Sec. III C, the long distance behavior of $\chi_A(\mathbf{r}_j, \mathbf{r}_{j'})$ can be related to the momentum dependence of the static correlation function $\tilde{\chi}^{ab}(\mathbf{q}, 0)$ in the amplitude channel $a = b = 1$ for small \mathbf{q} , which has the general form

$$\tilde{\chi}^{11}(\mathbf{q}, 0) \propto \frac{1}{J_{\alpha\beta}^A q_\alpha q_\beta + m_A^2}. \quad (75)$$

The magnetic coherence length is then given by

$$\xi_A = \sqrt{J_A}/(2m_A), \quad (76)$$

where $J_A = (J_{xx}^A J_{yy}^A - J_{xy}^A J_{yx}^A)^{\frac{1}{2}}$.

The constant C in Eq. (74) can be estimated by considering the Hubbard model with pure nearest neighbor hopping (with amplitude $-t$) at half-filling. At strong coupling (large U) the spin degrees of freedom are then described by the antiferromagnetic Heisenberg model, which exhibits a Néel ordered ground state with a magnetization reduced by a factor $n_0 \approx 0.6$ compared to the mean-field value [51]. On the other hand, evaluating the RPA expressions for the Hubbard model in the strong coupling limit, one recovers the mean-field results for the spin stiffness and spin wave velocity of the Heisenberg model with an exchange coupling $J_H = 4t^2/U$, namely $J = J_H/4$ and $c_s = \sqrt{2}J_H$. Evaluating the RPA spin amplitude correlation function yields $\xi_A = 1/\sqrt{8}$ in this limit. With the ansatz (74), one then obtains $n_0 = 1 - 4C/\pi$. Matching this with the numerical result $n_0 \approx 0.6$ yields $C \approx 0.3$ and $\Lambda_{uv} \approx 0.9$.

We finally note that we are not overcounting any fluctuations in our theory. In general, the electron fractionalization in Eq. (3) introduces redundant degrees of freedom associated with the gauge symmetry, Eq. (4). We have not explicitly fixed a gauge but, due to our (renormalized) mean-field treatment of the chargons, fluctuations of the magnetic order parameter are captured exclusively by the spinons.

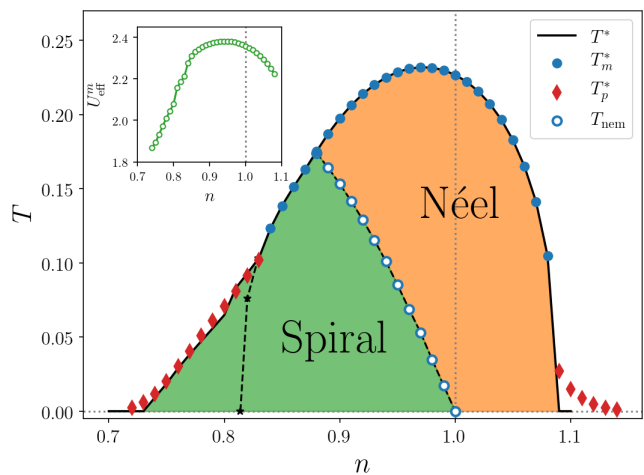


Figure 2. Pseudocritical temperatures T^* and nematic transition temperature T_{nem} as a function of density n . The symbols labeled by T_m^* and T_p^* indicate the temperatures at which the effective interaction diverges, in the magnetic or in the pairing channel, respectively. The black solid line labeled by T^* indicates the onset of magnetic order of the chargons and thus the boundary of the pseudogap regime in the absence of superconductivity. T^* coincides with the divergence temperature T_m^* for densities where the vertex diverges in the magnetic channel, and in the hole doped regime it is only slightly lower than T_p^* when the leading divergence occurs in the pairing channel. The labels “Néel” and “Spiral” refer to the type of chargon order. The dashed black line indicates a topological transition of the quasiparticle Fermi surface within the spiral regime. The inset shows the irreducible magnetic effective interaction U_{eff}^m as a function of density.

V. RESULTS

In this section we present and discuss results obtained from our theory for the two-dimensional Hubbard model, both in the hole- ($n < 1$) and electron-doped ($n > 1$) regime. We allow for next and second nearest neighbor hopping with amplitudes $-t$ and $-t'$, respectively, and we fix the ratio of the hopping amplitudes as $t'/t = -0.2$, and we choose a moderate interaction strength $U = 4t$. The energy unit is t in all plots.

A. Chargon mean-field phase diagram

The critical temperatures T_m^* and T_p^* at which the vertex $V^T(\mathbf{k}_1, \mathbf{k}_2, \mathbf{k}_3, \mathbf{k}_4)$ diverges are shown in Fig. 2. In a density range from $n \approx 0.83$ to $n \approx 1.08$, the divergence of the vertex is due to a magnetic instability. Beyond the edges of this density interval, the leading instability occurs in the d -wave pairing channel. Pairing extends into the magnetic regime at lower temperatures (below T_m^*) as a secondary instability. Vice versa, magnetic order is possible at temperatures below T_p^* in the regime where pairing fluctuations dominate [16, 30].

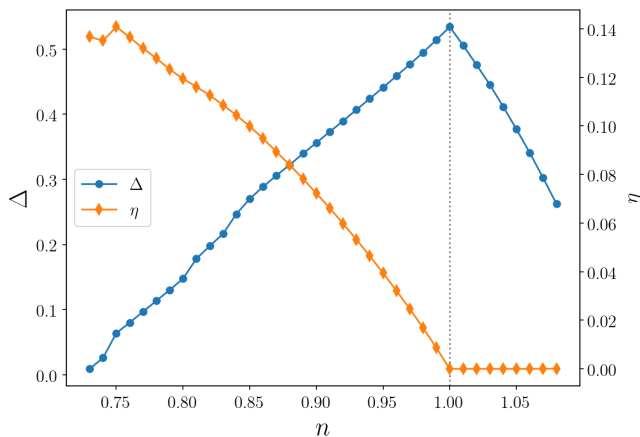


Figure 3. Magnetic gap Δ (left axis) and incommensurability η (right axis) at $T = 0$ as functions of the density.

In Fig. 2, we also show the irreducible effective magnetic interaction U_{eff}^m defined in Sec. III B. The effective interaction U_{eff}^m is strongly reduced from its bare value ($U = 4t$) by the non-magnetic channels in the fRG flow, while its density dependence is not very strong.

From now on we ignore the pairing instability and focus on the magnetic order of the chargons. We compute the magnetic order parameter Δ together with the optimal wave vector \mathbf{Q} as described in Sec. III B. In Fig. 3, we show results for Δ in the ground state ($T = 0$) as a function of the filling. We find a stable magnetic solution extending deep into the hole doped regime down to $n \approx 0.73$. On the electron doped side magnetic order terminates abruptly already at $n \approx 1.08$. This pronounced electron-hole asymmetry and the discontinuous transition on the electron doped side has already been observed in previous fRG+MF calculations for a slightly weaker interaction $U = 3t$ [30].

The onset temperature T^* for magnetic order of the chargons as obtained from the renormalized mean-field theory is shown in Fig. 2. At densities where magnetic interactions dominate, it coincides with the temperature T_m^* at which V^T diverges. At densities where the interaction diverges in the pairing channel, T^* is lying only slightly below T_p^* on the hole doped side, while it vanishes on the electron doped side. While the magnetic gap in the ground state reaches its peak at $n = 1$, as expected, the pseudocritical temperature T^* and the irreducible effective interaction U_{eff}^m exhibit their maximum in the hole doped regime slightly away from half-filling.

The magnetic states are either Néel type or spiral with a wave vector of the form $\mathbf{Q} = (\pi - 2\pi\eta, \pi)$, or symmetry related, with an “incommensurability” $\eta > 0$. In Fig. 3 results for η in the ground state are shown as a function of the density. At half-filling and in the electron doped region only Néel order is found, as expected and in agreement with previous fRG+MF studies [30]. Hole doping instead immediately leads to a spiral ground state with $\eta > 0$. Whether the Néel state persists at small hole

doping depends on the hopping parameters and the interaction strength. Its instability toward a spiral state is favored by a larger interaction strength [29]. Indeed, in a previous fRG+MF calculation at weaker coupling the Néel state was found to survive up to about 10 percent hole doping [30].

At low and moderate hole doping, there is a transition between a Néel state at high temperatures and a spiral state at low temperatures. Since the spiral state breaks the tetragonal symmetry of the square lattice, spiral order entails electronic nematicity. In Fig. 2 we show the corresponding nematic transition temperature T_{nem} as a function of density. T_{nem} merges with T^* at $n \approx 0.88$. For lower densities the magnetic order is spiral with $\eta > 0$ at any temperature below the magnetic transition temperature. Within the spiral regime there is a topological transition of the quasiparticle Fermi surface (indicated by the black dashed line in Fig. 2), where hole pockets merge. The Fermi surface extracted from the single-particle spectral function develops Fermi arcs on the right hand side of this transition, while it resembles the large bare Fermi surface on the left (see Sec. V C).

B. Spinon fluctuations

Once the magnetic order parameter Δ of the chargons and the wave vector \mathbf{Q} have been computed, we are in the position to calculate the NL σ M parameters from the expressions presented in Sec. III C.

In Fig. 4, we plot results for the spatial and temporal spin stiffnesses $J_{\alpha\alpha}^a$ and Z^a in the ground state. In the spiral state (for $n < 1$) out-of-plane and in-plane stiffnesses are distinct, while in the Néel state (for $n \geq 1$) they coincide. Actually the order parameter defines an axis, not a plane, in the latter case. All the quantities except Z^\square exhibit pronounced jumps between half-filling and infinitesimal hole-doping. These discontinuities are due to the appearance of hole pockets around the points $(\frac{\pi}{2}, \frac{\pi}{2})$ in the Brillouin zone [43]. The spatial stiffnesses are almost constant over a broad range of hole-doping, with a small spatial anisotropy $J_{xx}^a \neq J_{yy}^a$. The temporal stiffnesses Z^a exhibit a stronger doping dependence. The peak of Z^\perp at $n \approx 0.79$ is associated with a van Hove singularity of the quasiparticle dispersion [43]. On the electron doped side all stiffnesses decrease almost linearly with the electron filling. The off-diagonal spin stiffnesses J_{xy}^a and J_{yx}^a vanish both in the Néel state and in the spiral state with $\mathbf{Q} = (\pi - 2\pi\eta, \pi)$ and symmetry related.

In Fig. 5 we show the magnetic coherence length ξ_A and the average spin wave velocity c_s in the ground state. The coherence length is rather short and only weakly doping dependent from half-filling up to 15 percent hole-doping, while it increases strongly toward the spiral-to-paramagnet transition on the hole-doped side. On the electron-doped side it almost doubles from half-filling to infinitesimal electron doping. This jump is due to the for-

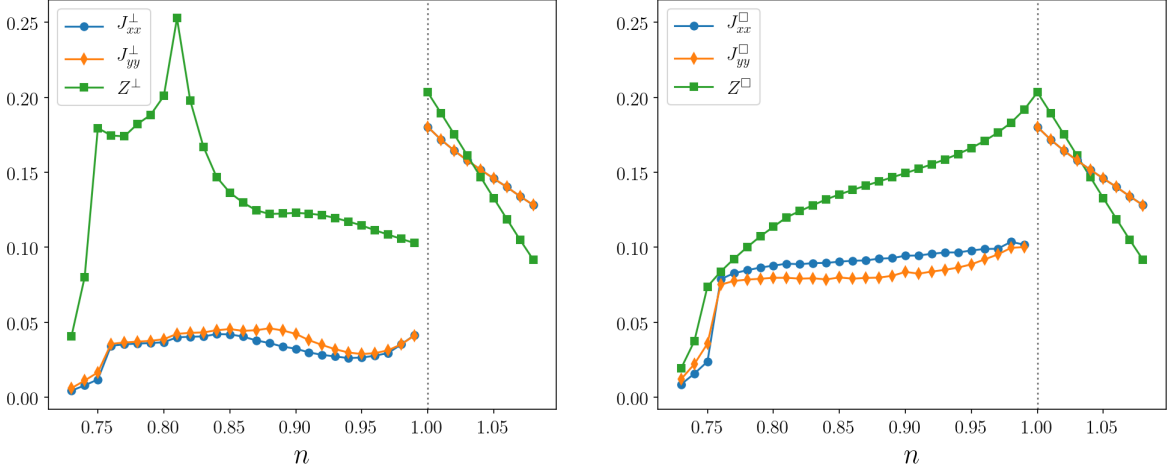


Figure 4. Out-of-plane (left panel) and in-plane (right panel) spatial (J) and temporal (Z) spin stiffnesses in the ground state ($T = 0$) as functions of the filling n . In the Néel state (for $n \geq 1$) out-of-plane and in-plane stiffnesses coincide.

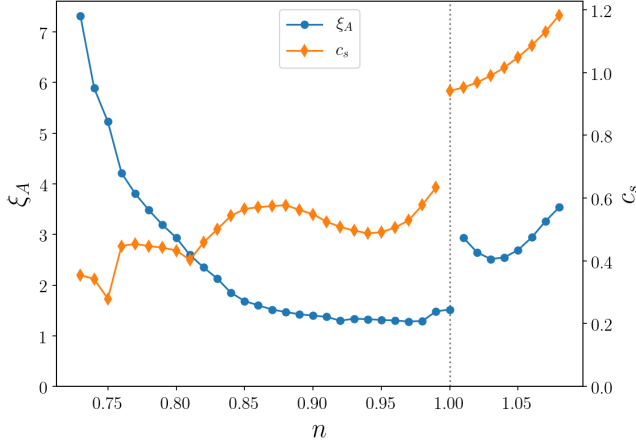


Figure 5. Magnetic coherence length ξ_A (left axis) and average spin wave velocity c_s in the ground state as functions of the filling n .

mation of electron pockets upon electron doping. Note that ξ_A does not diverge at the transition to the paramagnetic state on the electron doped side, as this transition is first order. The average spin wave velocity exhibits a pronounced jump at half-filling, which is inherited from the jumps of $J_{\alpha\alpha}^\perp$ and Z^\perp . Besides this discontinuity it does not vary much as a function of density.

We now investigate whether the magnetic order in the ground state is destroyed by quantum fluctuations or not. To this end we compute the boson condensation fraction n_0 as obtained from the large- N expansion of the NL σ M. This quantity depends on the ultraviolet cutoff Λ_{uv} . As a reference point, we may use the half-filled Hubbard model at strong coupling, as discussed in Sec. IV C, which yields $\Lambda_{uv} \approx 0.9$, and the constant in the ansatz Eq. (74) is thereby fixed to $C \approx 0.3$.

In Fig. 6 we show the condensate fraction n_0 com-

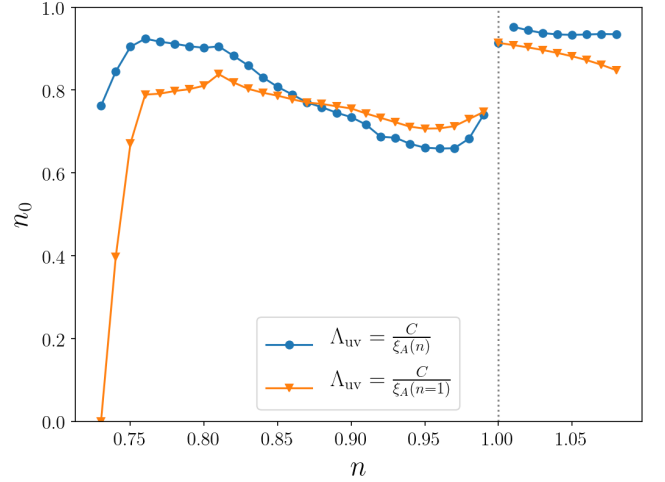


Figure 6. Fraction of condensed z -bosons n_0 at $T = 0$ for two distinct choices of the ultraviolet cutoff Λ_{uv} as a function of the filling.

puted with two distinct choices of the ultraviolet cutoff: $\Lambda_{uv} = \Lambda_{uv}(n) = C/\xi_A(n)$ and $\Lambda_{uv} = C/\xi_A(n = 1)$. For the former choice the cutoff vanishes at the edge of the magnetic region on the hole-doped side, where ξ_A diverges. One can see that n_0 remains finite for both choices of the cutoff in nearly the entire density range where the chargons order. Only near the hole-doped edge of the magnetic regime, n_0 vanishes slightly above the mean-field transition point, if the ultraviolet cutoff is chosen as density independent. The discontinuous drop of n_0 upon infinitesimal hole doping is due to the corresponding drop of the out-of-plane stiffness, while the discontinuous increase of n_0 upon infinitesimal electron doping, for the density dependent cutoff choice $\Lambda_{uv}(n) = C/\xi_A(n)$, is due to the discontinuity of $\xi_A(n)$. In the weakly hole-

doped region there is a substantial reduction of n_0 below one, for both choices of the cutoff. Except for the edge of the magnetic region on the hole-doped side, the choice of the cutoff has only a mild influence on the results, and the condensate fraction remains well above zero. Hence, we can conclude that the ground state of the Hubbard model with a moderate coupling $U = 4t$ is magnetically ordered over wide density range. The spin stiffness is sufficiently large to protect the magnetic order against quantum fluctuations of the order parameter.

C. Electron spectral function

Fractionalizing the electron operators as in Eq. (3), the electron Green's function assumes the form

$$\begin{aligned} [\mathcal{G}_{jj'}^e(\tau)]_{\sigma\sigma'} &= -\langle c_{j'\sigma'}(\tau)c_{j\sigma}^*(0) \rangle \\ &= -\langle [R_{j'}(\tau)]_{\sigma's'} [R_j^*(0)]_{\sigma s} \psi_{j's'}(\tau)\psi_{js}^*(0) \rangle. \end{aligned} \quad (77)$$

To simplify this expression, we decouple the average $\langle RR^*\psi\psi^* \rangle$ as $\langle RR^* \rangle \langle \psi\psi^* \rangle$, yielding [9, 10, 14]

$$[\mathcal{G}_{jj'}^e(\tau)]_{\sigma\sigma'} = -\langle [R_{j'}(\tau)]_{\sigma's'} [R_j^*(0)]_{\sigma s} \rangle \langle \psi_{j's'}(\tau)\psi_{js}^*(0) \rangle. \quad (78)$$

The spinon Green's function can be computed from the NL σ M in the continuum limit. Using the Schwinger boson parametrization (61), we obtain, in the large N limit,

$$\begin{aligned} \langle [R(\mathbf{r}_{j'}, \tau)]_{\sigma's'} [R^*(\mathbf{r}_j, 0)]_{\sigma s} \rangle &= -D(\mathbf{r}_j - \mathbf{r}_{j'}, \tau) \delta_{\sigma\sigma'} \delta_{ss'} \\ &\quad + n_0 \delta_{\sigma s} \delta_{\sigma's'}. \end{aligned} \quad (79)$$

The boson propagator $D(\mathbf{r}, \tau)$ is the Fourier transform of

$$D(\mathbf{q}, \omega_n) = \frac{1}{Z^\perp \omega_n^2 + J_{\alpha\beta}^\perp q_\alpha q_\beta + Z^\perp m_s^2}, \quad (80)$$

with the bosonic Matsubara frequency $\omega_n = 2\pi nT$. Fourier transforming Eq. (78), the electron Green's function is obtained in momentum representation as

$$\begin{aligned} \mathcal{G}^e(\mathbf{k}, \mathbf{k}', \nu_n) &= -T \sum_{\omega_m} \int_{\mathbf{q}} \text{tr} [\mathcal{G}(\mathbf{k} - \mathbf{q}, \mathbf{k}' - \mathbf{q}, \nu_n - \omega_m)] \\ &\quad \times D(\mathbf{q}, \omega_m) \mathbb{1} + n_0 \mathcal{G}(\mathbf{k}, \mathbf{k}', \nu_n), \end{aligned} \quad (81)$$

where $\mathcal{G}(\mathbf{k}, \mathbf{k}', \nu_n)$ is the chargin Green's function.

We see that when $n_0 = 0$, the electron Green's function is diagonal in momentum, that is, it is translational invariant, as the diagonal components of the chargin Green's function entering the trace are nonzero only for $\mathbf{k} = \mathbf{k}'$. Furthermore, in this case \mathcal{G}^e is proportional to the unity matrix in spin space, since there is no spin SU(2) symmetry breaking, and is thus given by a single normal state Green's function $G^e(\mathbf{k}, \nu_n)$. Performing the Matsubara sum in Eq. (81) and continuing to real frequencies, we get

$$\begin{aligned} G^e(\mathbf{k}, \omega) &= \sum_{\ell=\pm} \sum_{p=\pm} \int_{|\mathbf{q}| \leq \Lambda_{uv}} \frac{1}{4Z^\perp \omega_{\mathbf{q}}^{\text{SP}}} \left(1 + \ell \frac{h_{\mathbf{k}-\mathbf{q}}}{e_{\mathbf{k}-\mathbf{q}}} \right) \\ &\quad \times \frac{f(pE_{\mathbf{k}-\mathbf{q}}^\ell) + n_B(\omega_{\mathbf{q}}^{\text{SP}})}{\omega + i0^+ - E_{\mathbf{k}-\mathbf{q}}^\ell + p\omega_{\mathbf{q}}^{\text{SP}}} + \{\mathbf{k} \rightarrow -\mathbf{k}\}, \end{aligned} \quad (82)$$

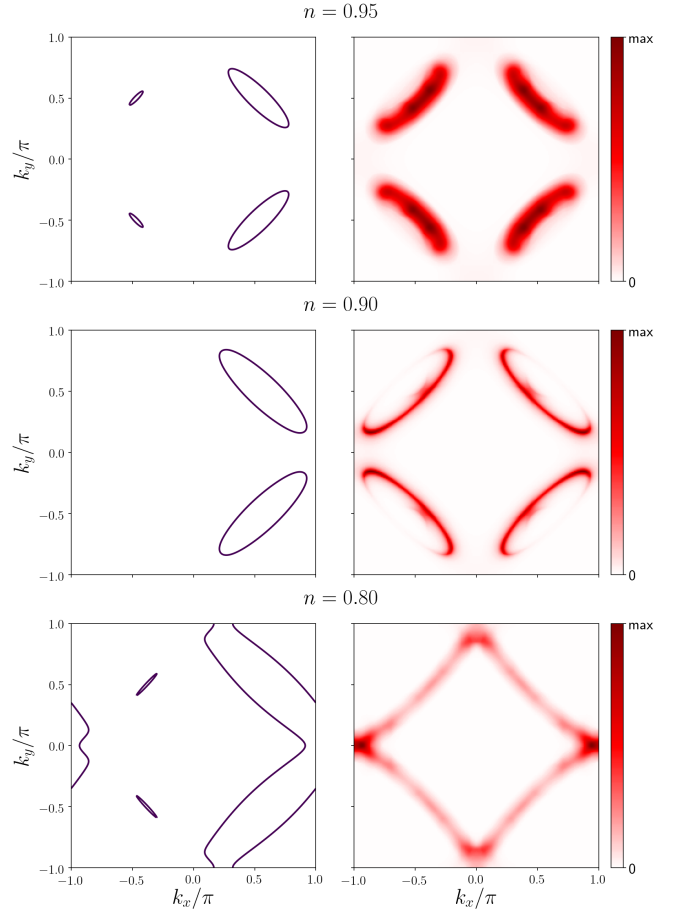


Figure 7. Quasiparticle Fermi surfaces defined as zeros of the chargin quasiparticle energies $E_{\mathbf{k}}^\pm$ (left column) and momentum dependence of electron spectral function at zero frequency (right column) for various electron densities. The temperature is $T = 0.05t$.

where

$$\omega_{\mathbf{q}}^{\text{SP}} = \sqrt{(J_{\alpha\beta}^\perp q_\alpha q_\beta) / Z^\perp + m_s^2}, \quad (83)$$

and $n_B(x) = (e^{x/T} - 1)^{-1}$ is the Bose distribution function.

In the right column of Fig. 7 we show the spectral function obtained as the imaginary part of the retarded electron Green's function at zero frequency as a function of momentum for various electron densities in the hole doped regime. The temperature $T = 0.05t$ is below the chargin ordering temperature in all cases. The Fermi surface topology is the same as the one obtained from a mean field approximation of spiral spin density wave order [52]. At low hole doping it originates from a superposition of hole pockets (see left column of Fig. 7), where the spectral weight on the back sides is drastically suppressed by coherence factors, so that only the front sides are visible. The spinon fluctuations lead to a broadening of the spectral function, so that the Fermi surface is smeared out. Since the spinon propagator does not

depend on the fermionic momentum, the broadening occurs uniformly in the entire Brillouin zone. Hence, the backbending at the edges of the “arcs” obtained in our theory for $n = 0.9$ is more pronounced than experimentally observed in cuprates. The backbending edges could be further suppressed by including a momentum dependent self-energy which has a larger imaginary part in the antinodal region [53].

VI. CONCLUSIONS

We have presented a SU(2) gauge theory of fluctuating magnetic order in the two-dimensional Hubbard model. The theory is based on a fractionalization of the electron operators in chargons and spinons [12–15]. The chargons are treated in a renormalized mean-field theory with effective interactions obtained from a functional renormalization group flow. They undergo Néel or spiral magnetic order in a broad density range around half-filling below a density dependent temperature T^* . Fluctuations of the spin orientation are described by a non-linear sigma model obtained from a gradient expansion of the spinon degrees of freedom. The parameters of the sigma model, the spin stiffnesses, have been computed from a renormalized RPA. Our approximations are applicable for a weak or moderate Hubbard interaction U . While magnetic long-range order of the electrons is still possible in the ground state, at any finite temperature the spinon fluctuations prevent long-range order – in agreement with the Mermin-Wagner theorem. We expect that at strong coupling even the ground state becomes disordered already at relatively low hole-doping, since fluctuations are then enhanced due to the shorter magnetic coherence length.

In spite of the moderate interaction strength chosen in our explicit calculations, the phase with magnetic chargin order below T^* exhibits all important features characterizing the pseudogap regime in high- T_c cuprates. The Fermi surface reconstruction yields a reduction of the electronic density of states. At low hole doping the Fermi surface obtained from the spectral function for single-particle excitations looks like Fermi arcs. The spinon fluctuations generate a spin gap at any finite temperature. The spinon fluctuations do not contribute to quantities involving only charge degrees of freedom, such as the longitudinal or Hall conductivities. It was already shown previously that Néel or spiral order of the chargons can explain the drastic charge carrier drop observed at the onset of the pseudogap regime in hole-doped cuprates [32, 52, 54–58].

In the Néel regime, the structure of our theory is very similar to the SU(2) gauge theory of the pseudogap phase derived by Sachdev and coworkers [7–11, 15]. Besides our extension to spiral states, the major new aspect of our work is that we *compute* the magnetic order parameter and spin stiffnesses instead of fitting the parameters of the theory. This computation revealed in particular an important particle-hole asymmetry of the stiffnesses.

Spiral order of the chargons entails nematic order of the electrons. At low hole doping, the chargons form a Néel state at T^* , and a spiral state at a lower temperature T_{nem} . The electrons thus undergo a nematic phase transition at a critical temperature *below* the pseudogap temperature. Evidence for a nematic transition at a temperature $T_{\text{nem}} < T^*$ has been found recently in slightly underdoped YBCO [59]. For large hole doping instead, the nematic transition occurs right at T^* , while nematic order is completely absent for electron doping, that is, above half-filling.

In the ground state of the two-dimensional Hubbard model there is a whole zoo of possible magnetic ordering patterns, and away from half filling Néel or spiral order do not always minimize the ground state energy. The most important competitor is stripe order, that is, collinear spin order associated with charge order, where holes accumulate in one-dimensional lines [3]. Stripe order in the ground state has been established rather convincingly for special cases, such as pure nearest neighbor hopping and doping concentration 1/8 [60]. The energy difference between distinct order patterns can be very small. At finite temperatures, the issue of the proper choice of the magnetic order reappears for the chargons. A classification of the numerous possibilities has been provided recently by Sachdev et al. [61]. We have focused on Néel and spiral states because any other state leads to a fractionalization of the Fermi surface into numerous tiny pieces (infinitely many for incommensurate wave vectors), which is in conflict with the experimental observation of only four arcs in the pseudogap phase of cuprates. Moreover, it is hard to explain the sharp carrier drop observed at the edge of pseudogap regime in high magnetic fields via collinear magnetic order [62]. Hence, to us Néel or spiral order of the chargons seems the most promising starting point to understand the universal features of the pseudogap phase. Refinements are required to capture also secondary instabilities, that is, charge order and superconductivity.

At finite temperatures, we obtain a “pseudogap” phase with a reconstructed Fermi surface and a spin gap also for the electron doped Hubbard model. In contrast, in electron doped cuprates one observes a comparatively broad (in doping) Néel phase, and no or only a very narrow pseudogap regime. Néel order at finite temperature is possible due to the interlayer coupling in cuprates. On the hole doped side, interlayer coupling stabilizes the Néel state only in a very narrow regime near half-filling. This electron-hole asymmetry can be explained by the asymmetry of the spin stiffnesses, which are much smaller on the hole doped side (see Fig. 4), enhancing thus the impact of spin fluctuations.

ACKNOWLEDGEMENTS

We are very grateful to Andres Greco, Elio König and Demetrio Vilardi for valuable discussions.

Appendix A: Linear term in the gauge field

In this Appendix we show that the linear term in Eq. (12) vanishes. Fourier transforming the vertex and the expectation value, the coefficient \mathcal{B}_μ^a can be written as

$$\mathcal{B}_\mu^a = \frac{1}{2} \int_{\mathbf{k}} T \sum_{\nu_n} \gamma_\mu^{(1)}(\mathbf{k}) \text{Tr} [\sigma^a \mathcal{G}(\mathbf{k}, \mathbf{k}, \nu_n)]. \quad (\text{A1})$$

Inserting \mathcal{G} from Eq. (52) one immediately sees that $\mathcal{B}_\mu^1 = \mathcal{B}_\mu^2 = 0$ for $\mu = 0, 1, 2$, and $\mathcal{B}_0^3 = 0$, too. Performing the Matsubara sum for \mathcal{B}_α^3 with $\alpha = 1, 2$, we obtain

$$\mathcal{B}_\alpha^3 = \frac{1}{2} \int_{\mathbf{k}} \sum_{\ell=\pm} [(\partial_{k_\alpha} \epsilon_{\mathbf{k}}) u_{\mathbf{k}}^\ell f(E_{\mathbf{k}}^\ell) + (\partial_{k_\alpha} \epsilon_{\mathbf{k}+\mathbf{Q}}) u_{\mathbf{k}}^{-\ell} f(E_{\mathbf{k}}^\ell)], \quad (\text{A2})$$

where $u_{\mathbf{k}}^\ell = \frac{1}{2}(1 + \ell h_{\mathbf{k}} / \sqrt{h_{\mathbf{k}}^2 + \Delta^2})$ with $h_{\mathbf{k}} = \frac{1}{2}(\epsilon_{\mathbf{k}} - \epsilon_{\mathbf{k}+\mathbf{Q}})$. One can see by direct calculation that this term vanishes if $\partial F(\mathbf{Q})/\partial \mathbf{Q}$ with $F(\mathbf{Q})$ given by Eq. (30) vanishes. Hence, \mathcal{B}_α^3 vanishes if \mathbf{Q} minimizes the free energy. A similar result has been obtained in Ref. [26].

Appendix B: Derivation of the NL σ M

Here we derive the NL σ M action (18) from Eq. (12). We first prove the identity

$$\partial_\mu \mathcal{R} = -i \mathcal{R} \Sigma^a A_\mu^a, \quad (\text{B1})$$

where \mathcal{R} is defined by Eq. (17), and Σ^a are the generators of the SU(2) in the adjoint representation,

$$\Sigma_{bc}^a = -i \varepsilon^{abc}, \quad (\text{B2})$$

with ε^{abc} the Levi-Civita tensor. Rewriting Eq. (17) as

$$\mathcal{R}^{ab} = \frac{1}{2} \text{Tr} [R^\dagger \sigma^a R \sigma^b], \quad (\text{B3})$$

we obtain the derivative of \mathcal{R} in the form,

$$\begin{aligned} \partial_\mu \mathcal{R}^{ab} &= \text{Tr} [R^\dagger \sigma^a (\partial_\mu R) \sigma^b] = \text{Tr} [R^\dagger \sigma^a R R^\dagger (\partial_\mu R) \sigma^b] \\ &= -i \mathcal{R}^{ac} \Sigma_{cb}^d A_\mu^d, \end{aligned} \quad (\text{B4})$$

which is the identity in (B1).

We now aim to express the object $\frac{1}{2} \mathcal{J}_{\mu\nu}^{ab} A_\mu^a A_\nu^b$ in terms of the matrix field \mathcal{R} . We write the stiffness matrix in terms of a new matrix $\mathcal{P}_{\mu\nu}$ via

$$\mathcal{J}_{\mu\nu}^{ab} = \text{Tr} [\mathcal{P}_{\mu\nu}] \delta_{ab} - \mathcal{P}_{\mu\nu}^{ab} = \text{Tr} [\mathcal{P}_{\mu\nu} \Sigma^a \Sigma^b]. \quad (\text{B5})$$

Using $\mathcal{R}^T \mathcal{R} = 1$, we obtain

$$\begin{aligned} \frac{1}{2} \mathcal{J}_{\mu\nu}^{ab} A_\mu^a A_\nu^b &= \frac{1}{2} \text{Tr} [\mathcal{P}_{\mu\nu} \Sigma^a \mathcal{R}^T \mathcal{R} \Sigma^b] A_\mu^a A_\nu^b \\ &= \frac{1}{2} \text{Tr} [\mathcal{P}_{\mu\nu} (\partial_\mu \mathcal{R}^T) (\partial_\nu \mathcal{R})], \end{aligned} \quad (\text{B6})$$

where we have used Eq. (B1) in the last line. The above equation yields Eq. (18). Relation (B5) can be easily inverted using $\text{Tr}[\mathcal{J}_{\mu\nu}] = 2 \text{Tr}[\mathcal{P}_{\mu\nu}]$.

Appendix C: Details on the large- N expansion

In this Appendix, we describe some details regarding the saddle point equations of the CP $^{N-1}$ action. Integrating out the z -bosons from Eq. (67), we obtain the effective action [46]

$$\begin{aligned} \mathcal{S}[\mathcal{A}_\mu, \lambda] &= N \int_{\mathcal{T}} dx \left[\ln(-2J_{\mu\nu}^\perp D_\mu D_\nu + i\lambda) - \frac{i}{2} \lambda \right. \\ &\quad \left. + \frac{1}{4} M_{\mu\nu} \mathcal{A}_\mu \mathcal{A}_\nu \right]. \end{aligned} \quad (\text{C1})$$

In the large N limit the functional integral for its partition function is dominated by its saddle point, which is determined by the stationarity equations

$$\frac{\delta \mathcal{S}}{\delta \mathcal{A}_\mu} = \frac{\delta \mathcal{S}}{\delta \lambda} = 0. \quad (\text{C2})$$

The first condition implies $\mathcal{A}_\mu = 0$, that is, in the large- N limit the U(1) gauge field fluctuations are totally suppressed. The variation with respect to λ gives, assuming a spatially uniform average value for λ ,

$$n_0 + T \sum_{\omega_n} \int_{\mathbf{q}} \frac{1}{Z^\perp \omega_n^2 + J_{\alpha\beta}^\perp q_\alpha q_\beta + i\langle \lambda \rangle} = 1, \quad (\text{C3})$$

where n_0 is the fraction of condensed bosons, which can be nonzero at $T = 0$. Performing the sum over the bosonic Matsubara frequencies $\omega_n = 2n\pi T$, inserting the identity

$$1 = \int_0^\infty d\epsilon \delta\left(\epsilon - \sqrt{J_{\alpha\beta}^\perp q_\alpha q_\beta / Z^\perp}\right), \quad (\text{C4})$$

and performing the \mathbf{q} -integral, we obtain Eq. (68) at $T > 0$ and Eq. (72) at $T = 0$.

[1] B. Keimer, S. A. Kivelson, M. R. Norman, S. Uchida, and J. Zaanen, From quantum matter to high-temperature superconductivity in copper oxides, *Nature* **518**, 179

(2015).

[2] C. Proust and L. Taillefer, The Remarkable Underlying Ground States of Cuprate Superconductors, *Annu. Rev.*

- Condens. Matter Phys.* **10**, 409 (2019).
- [3] M. Qin, T. Schäfer, S. Andergassen, P. Corboz, and E. Gull, The Hubbard Model: A Computational Perspective, *Annu. Rev. Condens. Matter Phys.* **13**, 275 (2022).
- [4] O. Gunnarsson, T. Schäfer, J. P. F. LeBlanc, E. Gull, J. Merino, G. Sangiovanni, G. Rohringer, and A. Toschi, Fluctuation Diagnostics of the Electron Self-Energy: Origin of the Pseudogap Physics, *Phys. Rev. Lett.* **114**, 236402 (2015).
- [5] T. Moriya and K. Ueda, Spin fluctuations and high temperature superconductivity, *Adv. Phys.* **49**, 555 (2000).
- [6] Y. M. Vilk and A.-M. S. Tremblay, Destruction of Fermi-liquid quasiparticles in two dimensions by critical fluctuations, *Europhys. Lett.* **33**, 159 (1996).
- [7] S. Sachdev and D. Chowdhury, The novel metallic states of the cuprates: Topological Fermi liquids and strange metals, *Prog. Theor. Exp. Phys.* **2016**, 12C102 (2016).
- [8] S. Chatterjee, S. Sachdev, and M. S. Scheurer, Intertwining Topological Order and Broken Symmetry in a Theory of Fluctuating Spin-Density Waves, *Phys. Rev. Lett.* **119**, 227002 (2017).
- [9] M. S. Scheurer, S. Chatterjee, W. Wu, M. Ferrero, A. Georges, and S. Sachdev, Topological order in the pseudogap metal, *Proc. Natl. Acad. Sci. USA* **115**, E3665 (2018).
- [10] W. Wu, M. S. Scheurer, S. Chatterjee, S. Sachdev, A. Georges, and M. Ferrero, Pseudogap and Fermi-Surface Topology in the Two-Dimensional Hubbard Model, *Phys. Rev. X* **8**, 021048 (2018).
- [11] S. Sachdev, Topological order, emergent gauge fields, and Fermi surface reconstruction, *Rep. Prog. Phys.* **82**, 014001 (2019).
- [12] H. Schulz, Functional Integrals for Correlated Electrons, in *The Hubbard Model*, edited by D. Baeriswyl (Plenum, New York, 1995).
- [13] N. Dupuis, Spin fluctuations and pseudogap in the two-dimensional half-filled Hubbard model at weak coupling, *Phys. Rev. B* **65**, 245118 (2002).
- [14] K. Borejsza and N. Dupuis, Antiferromagnetism and single-particle properties in the two-dimensional half-filled Hubbard model: A nonlinear sigma model approach, *Phys. Rev. B* **69**, 085119 (2004).
- [15] S. Sachdev, M. A. Metlitski, Y. Qi, and C. Xu, Fluctuating spin density waves in metals, *Phys. Rev. B* **80**, 155129 (2009).
- [16] J. Wang, A. Eberlein, and W. Metzner, Competing order in correlated electron systems made simple: Consistent fusion of functional renormalization and mean-field theory, *Phys. Rev. B* **89**, 121116(R) (2014).
- [17] P. M. Bonetti, Local Ward identities for collective excitations in fermionic systems with spontaneously broken symmetries (2022), [arXiv:2204.04132](https://arxiv.org/abs/2204.04132).
- [18] Z. Y. Weng, C. S. Ting, and T. K. Lee, Path-integral approach to the Hubbard model, *Phys. Rev. B* **43**, 3790 (1991).
- [19] W. Metzner, M. Salmhofer, C. Honerkamp, V. Meden, and K. Schönhammer, Functional renormalization group approach to correlated fermion systems, *Rev. Mod. Phys.* **84**, 299 (2012).
- [20] F. D. M. Haldane, Nonlinear Field Theory of Large-Spin Heisenberg Antiferromagnets: Semiclassically Quantized Solitons of the One-Dimensional Easy-Axis Néel State, *Phys. Rev. Lett.* **50**, 1153 (1983).
- [21] F. Haldane, Continuum dynamics of the 1-D Heisenberg antiferromagnet: Identification with the O(3) nonlinear sigma model, *Physics Letters A* **93**, 464 (1983).
- [22] P. Azaria, B. Delamotte, and T. Jolicoeur, Nonuniversality in helical and canted-spin systems, *Phys. Rev. Lett.* **64**, 3175 (1990).
- [23] P. Azaria, B. Delamotte, and D. Mouhanna, Low-temperature properties of two-dimensional frustrated quantum antiferromagnets, *Phys. Rev. Lett.* **68**, 1762 (1992).
- [24] P. Azaria, B. Delamotte, and D. Mouhanna, Spontaneous symmetry breaking in quantum frustrated antiferromagnets, *Phys. Rev. Lett.* **70**, 2483 (1993).
- [25] P. Azaria, B. Delamotte, F. Delduc, and T. Jolicoeur, A renormalization-group study of helimagnets in $D = 2 + \epsilon$ dimensions, *Nuclear Physics B* **408**, 485 (1993).
- [26] S. Klee and A. Muramatsu, SO(3) nonlinear σ model for a doped quantum helimagnet, *Nucl. Phys. B* **473**, 539 (1996).
- [27] P. A. Igoshev, M. A. Timirgazin, A. A. Katanin, A. K. Arzhnikov, and V. Y. Irkhin, Incommensurate magnetic order and phase separation in the two-dimensional Hubbard model with nearest- and next-nearest-neighbor hopping, *Phys. Rev. B* **81**, 094407 (2010).
- [28] R. Frésard, M. Dzierzawa, and P. Wölfle, Slave-Boson Approach to Spiral Magnetic Order in the Hubbard Model, *Europhys. Lett.* **15**, 325 (1991).
- [29] A. V. Chubukov and K. A. Musaelian, Magnetic phases of the two-dimensional Hubbard model at low doping, *Phys. Rev. B* **51**, 12605 (1995).
- [30] H. Yamase, A. Eberlein, and W. Metzner, Coexistence of Incommensurate Magnetism and Superconductivity in the Two-Dimensional Hubbard Model, *Phys. Rev. Lett.* **116**, 096402 (2016).
- [31] D. Vilaridi, C. Taranto, and W. Metzner, Dynamically enhanced magnetic incommensurability: Effects of local dynamics on nonlocal spin correlations in a strongly correlated metal, *Phys. Rev. B* **97**, 235110 (2018).
- [32] P. M. Bonetti, J. Mitscherling, D. Vilaridi, and W. Metzner, Charge carrier drop at the onset of pseudogap behavior in the two-dimensional Hubbard model, *Phys. Rev. B* **101**, 165142 (2020).
- [33] J. Berges, N. Tetradis, and C. Wetterich, Non-perturbative renormalization flow in quantum field theory and statistical physics, *Physics Reports* **363**, 223 (2002).
- [34] N. Dupuis, L. Canet, A. Eichhorn, W. Metzner, J. Pawłowski, M. Tissier, and N. Wschebor, The nonperturbative functional renormalization group and its applications, *Physics Reports* **910**, 1–114 (2021).
- [35] P. M. Bonetti, Accessing the ordered phase of correlated Fermi systems: Vertex bosonization and mean-field theory within the functional renormalization group, *Phys. Rev. B* **102**, 235160 (2020).
- [36] D. Vilaridi, P. M. Bonetti, and W. Metzner, Dynamical functional renormalization group computation of order parameters and critical temperatures in the two-dimensional Hubbard model, *Phys. Rev. B* **102**, 245128 (2020).
- [37] C. Honerkamp and M. Salmhofer, Temperature-flow renormalization group and the competition between superconductivity and ferromagnetism, *Phys. Rev. B* **64**, 184516 (2001).
- [38] C. Husemann and M. Salmhofer, Efficient parametriza-

- tion of the vertex function, Ω scheme, and the t, t' Hubbard model at van Hove filling, *Phys. Rev. B* **79**, 195125 (2009).
- [39] C. Husemann, K.-U. Giering, and M. Salmhofer, Frequency-dependent vertex functions of the (t, t') Hubbard model at weak coupling, *Phys. Rev. B* **85**, 075121 (2012).
- [40] D. Vilardi, C. Taranto, and W. Metzner, Nonseparable frequency dependence of the two-particle vertex in interacting fermion systems, *Phys. Rev. B* **96**, 235110 (2017).
- [41] D. Vilardi, C. Taranto, and W. Metzner, Antiferromagnetic and d -wave pairing correlations in the strongly interacting two-dimensional Hubbard model from the functional renormalization group, *Phys. Rev. B* **99**, 104501 (2019).
- [42] J. Lichtenstein, D. Sánchez de la Pëna, D. Rohe, E. Di Napoli, C. Honerkamp, and S. A. Maier, High-performance functional renormalization group calculations for interacting fermions, *Comput. Phys. Commun.* **213**, 100 (2017).
- [43] P. M. Bonetti and W. Metzner, Spin stiffness, spectral weight, and Landau damping of magnons in metallic spiral magnets, *Phys. Rev. B* **105**, 134426 (2022).
- [44] A. P. Kampf, Collective excitations in itinerant spiral magnets, *Phys. Rev. B* **53**, 747 (1996).
- [45] S. Sachdev, A. V. Chubukov, and A. Sokol, Crossover and scaling in a nearly antiferromagnetic Fermi liquid in two dimensions, *Phys. Rev. B* **51**, 14874 (1995).
- [46] A. Auerbach, *Interacting Electrons and Quantum Magnetism* (Springer-Verlag, New York, 1994).
- [47] A. V. Chubukov, S. Sachdev, and T. Senthil, Quantum phase transitions in frustrated quantum antiferromagnets, *Nuclear Physics B* **426**, 601 (1994).
- [48] P. Azaria, P. Lecheminant, and D. Mouhanna, The massive CP^{N-1} model for frustrated spin systems, *Nuclear Physics B* **455**, 648 (1995).
- [49] M. Campostrini and P. Rossi, The $1/N$ expansion of two-dimensional spin models, *Riv. Nuovo Cim.* **16**, 1 (1993).
- [50] A. V. Chubukov, T. Senthil, and S. Sachdev, Universal magnetic properties of frustrated quantum antiferromagnets in two dimensions, *Phys. Rev. Lett.* **72**, 2089 (1994).
- [51] E. Manousakis, The spin- $\frac{1}{2}$ Heisenberg antiferromagnet on a square lattice and its application to the cuprous oxides, *Rev. Mod. Phys.* **63**, 1 (1991).
- [52] A. Eberlein, W. Metzner, S. Sachdev, and H. Yamase, Fermi Surface Reconstruction and Drop in the Hall Number due to Spiral Antiferromagnetism in High- T_c Cuprates, *Phys. Rev. Lett.* **117**, 187001 (2016).
- [53] J. Mitscherling and W. Metzner, Non-Hermitian band topology from momentum-dependent relaxation in two-dimensional metals with spiral magnetism, *Phys. Rev. B* **104**, L201107 (2021).
- [54] J. G. Storey, Hall effect and Fermi surface reconstruction via electron pockets in the high T_c cuprates, *Europhys. Lett.* **113**, 2700 (2016).
- [55] J. G. Storey, Simultaneous drop in mean free path and carrier density at the pseudogap onset in high- T_c cuprates, *Supercond. Sci. Technol.* **30**, 104008 (2017).
- [56] S. Chatterjee, S. Sachdev, and A. Eberlein, Thermal and electrical transport in metals and superconductors across antiferromagnetic and topological quantum transitions, *Phys. Rev. B* **96**, 075103 (2017).
- [57] S. Verret, O. Simard, M. Charlebois, D. Sénéchal, and A.-M. S. Tremblay, Phenomenological theories of the low-temperature pseudogap: Hall number, specific heat, and Seebeck coefficient, *Phys. Rev. B* **96**, 125139 (2017).
- [58] J. Mitscherling and W. Metzner, Longitudinal conductivity and Hall coefficient in two-dimensional metals with spiral magnetic order, *Phys. Rev. B* **98**, 195126 (2018).
- [59] G. Grissonnanche, O. Cyr-Choinière, J. Day, R. Liang, D. A. Bonn, W. N. Hardy, N. Doiron-Leyraud, and L. Taillefer, No nematicity at the onset temperature of the pseudogap phase in the cuprate superconductor $YBa_2Cu_3O_y$ (2022), [arXiv:2205.05233](https://arxiv.org/abs/2205.05233).
- [60] B.-X. Zheng, C.-M. Chung, P. Corboz, G. Ehlers, M.-P. Qin, R. M. Noack, H. Shi, W. S. R., S. Zhang, and G. K.-L. Chan, Stripe order in the underdoped region of the two-dimensional Hubbard model, *Science* **358**, 1155 (2017).
- [61] S. Sachdev, H. D. Scammell, M. S. Scheurer, and G. Tarnopolsky, Gauge theory for the cuprates near optimal doping, *Phys. Rev. B* **99**, 054516 (2019).
- [62] M. Charlebois, S. Verret, A. Foley, O. Simard, D. Sénéchal, and A.-M. S. Tremblay, Hall effect in cuprates with an incommensurate collinear spin-density wave, *Phys. Rev. B* **96**, 205132 (2017).